University of Alberta

STUDIES ON MICROTUBULE MECHANICS

by

Chen Li

A thesis submitted to the Faculty of Graduate Studies and Research
in partial fulfillment of the requirements for the degree of

Master of Science

Department of Mechanical Engineering

Edmonton, Alberta
Spring 2008

Your file Votre référence
ISBN: 978-0-494-45842-6
Our file Notre référence
ISBN: 978-0-494-45842-6

Abstract

As the most rigid filaments of eukaryotic cytoskeleton, microtubules (MTs) are largely responsible for shape and mechanical rigidity of cells and are essentially involved in a range of functions such as cell division, cell motility and intracellular transport in eukaryotic cells. In this thesis, a novel thin-walled elastic beam model is suggested to study critical condition under which uniform bending of a flagellum will cause lateral/torsional buckling of the central pair MTs. The model predicts that bending-driven torsion of the central pair MTs does occur when the radius of curvature of the bent flagellum reduces to a moderate critical value typically of tens of microns, almost independently of the flagellum length; and the predicted wavelengths of the torsional buckling mode are insensitive to the flagellum length and comparable to some related experimental data. For the first time in the literature, these results indicate that torsion of the central pair MTs is inevitable under moderate conditions, as a result of bending-driven lateral buckling.

In addition, an orthotropic elastic shell model is used to study unexplained length-dependence of flexural rigidity and Young's modulus of MTs. It is shown that vibration frequencies and buckling load predicted by the present orthotropic shell model are much lower than that given by the existing isotropic beam model for shorter MTs, although the two models give almost identical results for sufficiently long MTs. In particular, much lower shear modulus and circumferential Young's modulus of MTs, which only weaken flexural rigidity of shorter MTs, are responsible for the observed length-dependence of the flexural rigidity. These results confirm that the observed length-dependence of the flexural rigidity and Young's modulus is a result of strongly anisotropic elastic properties of MTs which have a length-dependent weakening effect on flexural rigidity of shorter MTs.

Acknowledgements

I would like to extend my deepest gratitude and appreciation to Drs. Chongqing Ru and Andrew Mioduchowski for their invaluable guidance, support and encouragement that carried me on through difficult times and helped me in all the time of my graduate studies.

I am also grateful to my parents, my wife for their patience, love and support throughout my graduate studies.

Chen Li

Edmonton, Alberta

Fall 2007

Table of Contents

List of Figures

List of Tables

Chapter 1

Introduction

1.1 Background of the research

Biological science is always thought to be an integrated subject. With progress made in biological science and the engineering field, cell mechanics has become a research focus in recent years.

1.1.1 Cells, microtubules (MTs)

The cell is the basic unit of life. The vast diversity of living organisms is based on this single basic building block. Cells vary in size and shape. For example, the smallest cell has a diameter of no more than 0.2 μm while the largest cell has a diameter of 1 mm. Human cells usually have diameters in the range of 3-20 μm. From the point of view of cell types, all living cells can be classified into one of two general types: prokaryote and eukaryote [1, 2]. The eukaryotic cells have a major increase in complexity of organization, especially its cytoskeleton. The shape of eukaryotic cell is determined by its cytoskeleton, which is an internal framework of filaments. The various filaments have been classified into three types according to their diameter. They include microfilaments (5-7 nm), intermediate filaments (8-11 nm), and MTs (24-28 nm) as stated in [2]. It is this cytoskeleton network of filaments existing in every eukaryotic cell that becomes one of the most interesting biological objects from the point of view of nanophysics and molecular electronics [3]. While the three cytoskeleton filaments share general features, each also has its specific physical properties and structures, making them best suited to carry out specific tasks within the cell, and they often work together. For example, the microfilaments (also termed actin filaments) can be cross-linked by other proteins to form a wide variety of cellular structures and can produce force and generate cell movement. The essential function of intermediate filaments is to maintain correct tissue structure and

function of the cell. But, in our case we mainly focus on microtubule's structure and function in the cell.

The protein tubulin is the basic sub-unit that forms a microtubule. Tubulin molecules assemble with one another to form protofilaments and then they form microtubule tubes about $25\,nm$ in diameter. As stated by Portet et al. [4], MTs are long, hollow, cylindrical objects made up of protofilaments interacting laterally, and consisting of longitudinally stacked α and β tubulins (see Fig. 1.1). Within the cell, MTs are normally organized in an aster radiating near the nucleus towards the cell periphery and are highly dynamic polymers, characterizes by dynamic instabilities, successive periods of growth and shrinkage [5, 6].

MTs are the most rigid filaments of eukaryotic cytoskeleton [7-10], and are largely responsible for the shape and mechanical rigidity of cells, and are involved in a range of functions such as cell division, cell motility and intracellular transport in eukaryotic cells [11-14]. As stated by Scholey in [15], MTs can generate pushing and pulling forces as they grow and shrink by addition and loss of sub-units from their ends, and they also serve as tracks for motor proteins. At the single-molecule level, cytoskeletal proteins generate piconewton-scale forces and nanometer-scale movements, but during cell division, they are capable of generating forces in the range of nanonewtons and serve to accurately move intracellular components and rearrange areas of the cell surface over distances of tens of microns. These cytoskeletal proteins co-operate to drive the motility events underlying the mechanics and regulation of cell division. Therefore, MTs play very important roles during cell division. The basic principle of biology, in the cell theory of the 19^{th} century, is that cells can be produced only by the division of pre-existing cells. As a result, cell division and MTs' role in cell division has been paid much attention to by researchers. Regarding other functions of MTs, Lewin et al. [2] also discussed how MTs serve as tracks for motor proteins. They summarized that MTs almost always function together with the molecular motors that move on them. These motor proteins attach to various cargos, including organelles and vesicles, and pull them along the surface of the microtubule, much like trucks move cargos on a highway. Portet et al. [4] also mentioned that MTs are involved in a number of functions of the cell, such as cell shape maintenance and mitosis, and play an important role in intracellular transport. They

found that MTs form the mitotic spindles for the segregation of the chromosomes during cell division, and they are supports for directional transport driven by motor proteins.

In summary, each of the protein fibers has specific physical properties and structures suitable for its role in the cell. MTs are most important components in cell skeleton and all its structure features are right matched with their roles in the cell.

1.1.2 Flagella, "9+2" axoneme, central pair and doublets

Cells can move with respect to their environment such as a fluid medium. A common propulsion mechanism for cell movement employs flagella (Latin plural for whip) [9-11, 16, 17]. An interesting biological phenomenon is that cilia and flagella can move a cell as they beat.

Flagella are long whip-like organelles extending from the cell's body [18] (see Fig. 1.2), and have a typical length of about 10 microns, although examples of ten times of this length are known. A cell typically has one or two flagella, which are encased into the cell's membrane so that the interior of a flagellum is accessible to the cell's cytoplasm. Flagella are motile and wiggle to move the cell. Some cells bend their flagella to produce a wave-like motion, whereas others rotate them in a manner similar to a ship's propeller. Torque and thrust generated by flagella can propel a cell at up to a few tens of a micron per second [9-11, 16, 17] (see Fig. 1.3).

Here we introduce terminology to clarify. Both cilia and flagella are long appendages that extend from the cell body. When these structures occur together in large numbers they are usually referred to as cilia, and when they occur singly or in small numbers they are referred to as flagella. In either case, they have the same internal structure, and are composed of many of the same proteins and have the same intraflagellar transport system [18] even though cilia are much shorter than flagella in length. Therefore, for clarification, from this point forward, the term flagella is used.

From the point of view of flagella structure, each of these flagella is composed of a long bundle of MTs surrounded by an extension of the plasma membrane. When flagella bend, they beat back and front and move fluid past the surface of the cell. The question of where the motion is generated has attracted much attention from researchers. There are experimental manipulations showing that flagella will continue to beat if removed from

the cell, which demonstrates that the motion is generated within the flagella. The force is generated by the protein core of the flagellum, which leads to another biological structure - the axoneme. The protein core of a flagellum, the axoneme, is a highly ordered structure. The major structural feature of the axoneme is that the cross section is a precisely organized bundle of MTs which run continuously for the axoneme's entire length. Arranged in a circle are nine unusual doublet MTs, each composed of A and B tubule. At the center of the ring are two complete MTs. This characteristic arrangement of MTs within the axoneme is described as "9+2" structure. As stated by Rosenbaum et al. [18], the "9+2" axoneme contains nine doublet MTs (doublets) and two central MTs (central pair). In addition, the axoneme also contains inner and outer dynein arms, which generate the force for motility, and radial spokes and central pair projections, which regulate the motile machinery.

Returning to the question of how the flagella can move a cell as they beat, as mentioned above, flagella generate a beating motion by propagating a bend in the axoneme, and there is a bend in the central pair as well. Dyneins are activated sequentially both along the length and around the circumference of the axoneme in order to propagate the bend. Dyneins are regulated by the central pair MTs and the radial spokes. In some organism, the central pair rotates rapidly and as they spin may transmit signals to the radial spokes, which in turn activate dynein activity. So, the central pair plays an important role in moving cell by flagella bending.

On the other hand, in any discussion of the regulation of dynein arm activity by radial spoke-central pair MTs interactions, it should be noted that there is evidence suggesting that the central pair of MTs rotates within the ring of outer doublet MTs in many cells [19]. Indeed, the relationship between the central pair rotation and flagella bend has been discussed since 1979 by Omoto and Kung [20] to 2004 by Mitchell et al. [21]. They mentioned that the two MTs of the central pair are highly conserved structural elements of typical "9+2" eukaryotic flagella, but their function is still poorly understood. The central pair, therefore, provides important but at present uncharacterized functions to most flagella.

Microtubule doublets also play an important role in the periodic beating movement of the axoneme. They are structural components of axoneme and contain a number of

proteins besides tubules. Sui et al.[22] obtained a three dimension density map of the intact microtubule doublets by using cryo-electron tomography and image averaging in 2006. From the density map it can be seen that the microtubule doublet consists of a complete singlet microtubule, the A-tubule containing 13 protofilaments, and an incomplete microtubule, the B-tubule containing 10 protofilaments. Unlike singlet microtubule which is circular in cross-section, the A-tubules show a slight elliptical deformation with an elongation of about 8% in the axeneme's radial dimension. They analyzed the configuration of the proteins inside the microtubule doublets and suggested that the configuration of the proteins appears to be designed to stabilize and maintain the protofilament architecture of the doublets as it undergoes the stresses involved in axoneme motion and also to favor bending in the direction that corresponds to twisting of the axoneme. This will be a basis for quantitative modeling of mechanical properties. We are planning to model the doublets in our future work based on this structure configuration.

1.1.3 Developments in MT-mechanics and two worth-studying problems

Biomechanics is an integrated science, which integrates the laws of physics, human structural anatomy, and working concepts from engineering to describe the motion of the body and body segments. It is a scientific discipline concerned with understanding and improving human biological function and response as well as the biological function and response of other species [23]. Biomechanics have attracted more and more attention from scientists and researchers and also have had much more progress, especially in cell mechanics field.

As mentioned by Richard et al. [24], rapidly evolving and emerging techniques have afforded new opportunities to impart known mechanical conditions to cells, and to study their adaptive responses. The results of such studies have provided new insights into the biomechanics of tissues. If we look ahead to the future, we can speculate that more and more attention will be paid to structural networks existing within cell and investigate their responses to mechanical changes. All kinds of experiments and theoretical methods will need to be developed in order to ascertain the relationship of the mechanical environment and cell, tissue, and organ response.

As reviewed by Lim et al.[25], being physical entities, living cells possess specific structural and physical properties that enable them to withstand the physiological environment as well as mechanical stimuli occurring within and outside the cell body. Living cells in the human body are constantly subjected to mechanical stimulations throughout life. These stresses and strains can arise from both the external environment and internal physiological conditions. Cells can respond in a variety of ways depending on the magnitude, direction and distribution of mechanical stimuli. Studies have shown that many biological processes, such as growth and migration, are influenced by changes in cell's shape and structural integrity. In fact, any of these deviations in the structural and mechanical properties can result in the breakdown of these physiological functions and may lead to diseases because any deviation from these properties will not only undermine the physical integrity of the cells but also their biological functions. Therefore, a quantitative study in single cell mechanics will need to be conducted. In addition to experimental methods, some mechanical models have been developed to characterize mechanical responses of living cells when subjected to both transient and dynamic loads. It is for certain that more detailed and accurate mechanical models of living cells can be developed if we know more about structural features, appropriate constitutive relations for each of components within cells. As a matter of fact, there have already been a great deal of mechanical models applied in biomechanical phenomena. Just like Schoutens et al. summarized in [26] that the theory of elasticity has been applied to the movement of flagella by Machin (1958) and by Rikmenspoel (1965, 1966).

Based on development in biomechanics, many mechanical models such as continuum beam models and shell model have been widely used to analyze the mechanical behaviors of components within a cell. In the following, we will introduce two worth-studying research problems which are interpreted by a thin-wall beam model and an orthotropic shell model separately.

As the first worth-studying problem, we know from Section 1.1.2 that the relationship between torsion of the central pair and bending of flagella has been discussed for many years. The central pair is the component of "9+2" axoneme. The axoneme also contains inner and outer dynein arms, which generate the force for motility, and radial spokes and central pair projections, which regulate the motile machinery. How the central

pair regulate the motile mechanism is not clear and has been explored by many researchers. Omoto et al. [20] began to study this issue relatively earlier and found that the central pair rotates counter-clockwise 360° per beat cycle and this rotation may regulate the dynein arms. In the wake of that, the relationship between the torsion of the central pair and the bending of the flagella has been focused on, until now it is still a remarkable issue attracting considerable attention, leading to the first problem in the thesis: torsion of the central pair MTs in eukaryotic flagella due to bending-driven lateral buckling. In this thesis, we will investigate what causes the torsion of the central pair when the flagella are bending by a thin-wall beam model.

MTs are most important filaments of the eukaryotic cytoskeleton and they form the axoneme which is the moving core of flagella. They are thought to be responsible for cell shape, cell division, cell motility, and intercellular transport in eukaryotic cells. All these roles are structural and they require that MTs have sufficient resistance to bending. Meanwhile, MTs in living cells frequently bend and occasionally break, suggesting that relatively strong forces act on them as mentioned by Odde et al. [27]. These results suggest that the mechanical behaviors of MTs change in response to mechanical deformation. Whether MTs possess appropriate mechanical properties for these cellular functions such as maintaining cell shape makes the measurement of flexural rigidity of MTs become the focus of many research groups.

As the second worth-studying problem, however, a remarkable controversy has occurred and remained in the literature, regarding flexural rigidity and the associated Young's modulus of MTs because the flexural rigidity obtained from many different measurements has an unrelated spreading over a wide range. The reasons why the measured flexural rigidity is in such a large range should be from many factors, however, among various factors affecting the measured flexural rigidity, the length of MTs has been identified as a key parameter [28, 29]. Unlike the usual concept of length-independent flexural rigidity of elastic rods, it seems that MTs have a length-dependent flexural rigidity from the previous various researches, which leads to the second problem in the thesis: length-dependence of flexural rigidity as a result of anisotropic elastic properties of MTs. In this thesis, we will try to explore the unexplained

length-dependence of the flexural rigidity of MTs remained in previous literatures by an orthotropic shell model instead of isotropic beam model.

1.2 Statements of research problems

In Section 1.1.3, we introduced two worth-studying problems based on development in biomechanics. In this section, we will discuss the two research problems in detail.

1.2.1 Statements of the two research problems

In this thesis, we will focus on solving two problems mentioned in Section 1.1.3. The first problem is torsion of the central pair MTs in eukaryotic flagella due to bending-driven lateral buckling. Mechanical behaviors of flagella are crucial for their biological functions. So, sliding-bending mechanics of flagella [12, 26, 30-35], and related hydrodynamics of flagella in a fluid medium [16, 36-42] have been the focus of numerous earlier and recent experimental and theoretical researches. More recently, a remarkable issue which has attracted considerable attention is bending-related torsion of the central pair MTs of flagella [20, 21, 43-48]. The exact mechanism and functions of torsion of the central pair are not yet fully understood. Since the central pair is believed to play a vital role in regulation of flagella motion [49, 50], it is relevant to study the mechanism responsible for torsion of the central pair MTs in eukaryotic flagella.

The second problem is length-dependence of the flexural rigidity as a result of anisotropic elastic properties of MTs. As reviewed in Section 1.1, as the most rigid filaments of eukaryotic cytoskeleton [7-10], MTs are largely responsible for shape and mechanical rigidity of cells and are essentially involved in a range of functions such as cell division, cell motility and intracellular transport in eukaryotic cells [11-14]. In order to probe mechanical properties of MTs, continuum (isotropic) elastic beam models have been widely used to analyze 1D rod-like deformation of MTs, such as column-like buckling [28, 51] and beamlike vibration [52, 53], from which flexural rigidity of MTs [29, 54-58] and the Young's modulus were estimated. However, as mentioned in Section 1.1.3, a remarkable controversy has occurred and remained in the literature, regarding flexural rigidity and the associated Young's modulus of MTs. As stated recently by Kasas

et al. [52], "two decades of measurements involving different techniques... resulted in values of Young's modulus between 1 MPa (see [29, 54]) and 7 GPa (See [28, 29, 55])." Therefore, it is relevant to clarify why the estimated flexural rigidity from different MTs is scattered over such a wide range.

We also mentioned in Section 1.1.3 that, among various factors affecting the measured flexural rigidity, the length of MTs has been identified as a key parameter [28, 29]. The present work aims to quantitatively show that as modeled as an elastic beam, the flexural rigidity of MTs does depend on their length, as a result of strongly anisotropic elastic properties of MTs. An orthotropic shell model is used to examine this issue.

1.2.2 Overview of existing studies

For the first worth-studying problem, torsion of the central pair MTs in eukaryotic flagella due to bending-driven lateral buckling, we know from Section 1.1.2 that cells can move with respect to their environment such as a fluid medium. A common propulsion mechanism for cell movement employs flagella. But the role of the central pair in regulation of flagella motion remains unclear. Bending-related torsion of the central pair has gained considerable attention.

There are many studies on the role of central pair in regulation of flagella motion. Omoto et al. [20] found that the beat of a flagellum is typically three-dimensional movement, thus the dynein arms must be coordinated in their actions. However, the mechanism for coordination is not known. They suggested that the central pair rotates anti-clockwise 360° per beat cycle and this rotation may regulate the dynein arms. In their opinions, the central pair is an ideal candidate for at least part of this regulatory mechanism for several reasons. First, orientation of the central pair is correlated with beat direction. Second, various chlamydomonas mutants missing central pair are to be found paralyzed. Third, studies have indicated some interactions between radial spoke of the peripheral doublets and the projections from the central pair. So they speculated that the rotation of the central pair may generate the twist and cause its helical propagation toward the tip.

Two years later from 1979, Omoto et al. [43] stated that relatively little is known about the control mechanisms which coordinate the inter-doublet sliding and axonemal

bending to produce the effective motion observed in various flagella. This time they found that the central pair MTs undergoes continuous rotation in one direction. They suggested this rotation provides the motive force for the cell but they do not know what caused the central pair to rotate. So they speculated that one possibility is that the rotation is a passive response to 3-dimensional bending of the "9+2" axoneme of the flagellum. Alternatively, rotation may be the results of interactions between the radial spoke and the central sheath in the "9+2" region, or may be caused by a rotary motor in the axoneme. Although further studies will be necessary to determine the basis for the rotation, it has been proposed that the central pair undergo a systematic movement correlated with beat cycle and this movement is involved in regulating the flagella motion.

Two decades later from 1979, Omoto et al. [45] continued studying on this issue because mechanism and force for central pair rotation is still not clear. They concluded that there must be circumferential and longitudinal regulation of shear forces to produce effective bending motion of an axoneme. The central pair MTs are ideally situated to perform this regulatory function. But, what drives the central pair to rotate? This time they speculated that there are two general possibilities for what drives the rotation: one is that some enzymes, possibly kinesins, which have recently been found to be associated with the central pair, are actively rotating the central pair; the other is, the helical central pair is passively rotated by the bending of the axoneme. When the bend propagates distally, the helical shape will rotate to place the helix in the lowest energy position to conform to the bend.

Woolley et al. [44] studied whether the mechanical activity within the "9+2" axoneme of flagella can result in torsion of the axoneme, however they did not show what role the central pair plays in the torsion of axoneme and the relationship between the torsion of central pair and bending of flagella.

Mitchell's group started to study the issue of torsion of central pair in 2003[47], they tried to establish a relationship between flagellar bends and orientation of the central pair. They found that central pair orientation differs in bent regions and straight regions, its orientation changes 180° between principle and reverse bend. Although the fundamental reasons for this dichotomy between a fixed and a rotating central pair remain unresolved, the central pair rotation is most common and accepted by most researchers. In 2004,

Mitchell et al. [21] continued studying this problem. They thought that regulation of flagella motion depends on interactions between radial spoke and the central pair. Although the central pair does rotate during bend propagation in flagella, propulsive forces for central pair rotation are still unknown. But, they suggested that spoke-central pair interactions are not needed to generate torque for rotation and most likely the bend propagation drives central pair rotation.

Inspired by the above studies, we will try to explore the relationship between torsion of the central pair and bending of flagella.

The second worth-studying problem is length-dependence of the flexural rigidity as a result of anisotropic elastic properties of MTs. We know from Section 1.1.1 and 1.1.2 that MTs are most important filaments of the eukaryotic cytoskeleton and they are responsible for cell shape, cell division, cell motility, and intercellular transport in eukaryotic cells. All these roles require that MTs must have sufficient flexural rigidity to adapt to its roles and adjust its mechanical behaviors in response to mechanical deformation. So, the measurement of flexural rigidity of MTs has become the focus of many research groups.

Based on theory of strength of materials, we could directly measure the flexural rigidity of MTs by applying a small known force to one end of a clamped microtubule and measure its deflection and then obtain the flexural rigidity of the microtubule. But owing to the small size of the microtubule, such a method is technically difficult. Therefore, Gittes et al. [55] have measured the flexural rigidity of MTs by thermal bending. By measuring, the mean flexural rigidity of MTs is around $2.2\times10^{-23} N\cdot m^2$, the flexural rigidity of these MTs corresponds to a persistence length of $5200\,\mu m$, then if tubulin are homogeneous and isotropic, the microtubule's Young's modulus would be around 1.2 *GPa* .This was the first direct measurement of the flexural rigidity of MTs.

From then on, many researchers have been making every effort to get more accurate flexural rigidity of MTs by means of methods, including experimental methods and modeling methods during these years. For example, Venier et al. [54] use two independent methods to measure the flexural rigidity of MTs. One method is that a hydrodynamic flow was applied to MTs and the flexural rigidity was derived from the analysis of the bending shape of the MTs at equilibrium in the flow. The other is the

flexural rigidity was derived from the thermal fluctuation of the free end of axoneme-bound MTs. With both methods, the flexural rigidity of MTs is estimated as $(0.85 \pm 0.2) \times 10^{-23} N \cdot m^2$ which correspond to a persistence length of $2000 \pm 300 \mu m$. If assumed to be isotropic material, the Young's modulus of MTs would be around $0.5 \pm 0.1 GPa$.

The flexural rigidity of a single microtubule by direct buckling using the optical trapping technique was measured by Kurachi et al. [28]. Three ways of estimating the flexural rigidity of a continuous slender rod were used, one from the observed critical load of buckling and the other two from deflected lengths and angles of bending. Obtained values agreed well when applied to analysis of buckling MTs (see Fig. 1.4). The flexural rigidity is (3.4 to 12)$\times 10^{-23} N \cdot m^2$ for MAP-stabilized MTs with length (10 to 28) μm, and (0.13 to 0.86)$\times 10^{-23} N \cdot m^2$ for taxol-stabilized MTs with length (4 to 12) μm, which is a spread range over the length of MTs.

With techniques making progress, various methods are applied in measuring the flexural rigidity of MTs by many research groups. In 1996, Felgner et al. [59] used laser light directly to grab and bend MTs and then analyzed the bending of a microtubule and obtained that the flexural rigidity is between $1 \times 10^{-24} N \cdot m^2$ and $18 \times 10^{-24} N \cdot m^2$. At the same time, Elbaum et al. [60] studied buckling of MTs to measure the flexural rigidity of MTs. One measurement result is $EI = 2.6 \times 10^{-23} N \cdot m^2$, and the corresponding persistence length is 6300 μm. In 2002, Kis et al. [61] decided the mechanical anisotropy of a single microtubule by measuring the Young's Modulus and shear modulus. This is why MTs have a Young's modulus at least 2 orders of magnitude higher than the shear modulus.

Takasone et al. [29] also measured the flexural rigidity by using a laser trapping technique and dark-field microscopy but they still modeled microtubule as an elastic rod (see Fig. 1.5). Finally they obtained the flexural rigidity of MTs is $10^{-25} \sim 10^{-23} N \cdot m^2$ for the 5~25 μm length MTs. The effective Young's modulus of MTs with 5~20 μm length would be $50 \sim 10^3 MPa$ assuming that the MTs have the same modulus for compression and extension and that their cross section is constant over the entire length. Pablo et al. [62] probed the local mechanical properties of MTs at the nanometer scale by radial indentation with a scanning force microscope tip, combined with both thin-shell theory

and finite element methods. The Young's modulus was found to be around $1\,GPa$. Tuszynski et al. [63] reviewed and modeled the experimental parameters which characterize elastic properties of MTs and summarized that Young's modulus is (0.1 to 2.7) Gpa, flexural rigidity is (2.9 to 45)$\times 10^{-24}\,N\cdot m^2$ in previous research results. They obtained effective Young's modulus due to longitudinal compression is $1.32\,GPa$.

Until recently, Kitumoto et al. [58] still used direct buckling force measurements with optical traps to determine the flexural rigidity of MTs but they applied a new model assuming non-axial buckling. They obtained an EI of (1.9 to 8.5)$\times 10^{-24}\,N\cdot m^2$, and a Young's modulus of (0.12 to 0.46) GPa. At the same time, Pampaloni et al. [64] systematically studied mechanical properties of MTs and the dependence of persistence length on the length of MTs. Upon varying length between $2.6\,\mu m$ and $47.5\,\mu m$, they found a systematical increase of persistence length from $110\,\mu m$ to $5035\,\mu m$.

From the above values obtained, we can see that estimated flexural rigidity from different MTs is scattered over a wide range. Among the above measurements of flexural rigidity of MTs, there are several measurements that have to be focused on.

Kurachi et al. [28] measured the flexural rigidity of a single microtubule by direct buckling using the optical trapping technique. They found that the flexural rigidity of MTs is not a constant parameter defining the rigidity of a microtubule. They speculated that there may exist a three-dimensional superstructure which support the deviation of flexural rigidity analysis based on the homogeneous rods. The increase of flexural rigidity with length means that the longitudinal force required to buckle a microtubule does not decrease in proportion to the square of length as expressed in Euler beam model. This means that a microtubule is more resistant to a longitudinal compressive force than simply expected from isotropic rod theory as the microtubule grows longer. They concluded the length dependency of flexural rigidity on microtubule length. But they just speculated that such a unique property of microtubule may be of critical importance to their logical activity and did not give reasons.

But Felgner et al. [59] have a different point of view. Their results cannot confirm such length dependence. Furthermore, they think that the flexural rigidity should be a constant, by definition, for a rod–like polymer which is symmetric under translation along its long axial. Takasome et al. [29] have similar point of view with Kurachi et al.

They also found that the EI values they obtained for the deformation modes are functions of MTs length L. They interpreted that the different results of EI dependence on length L might be caused by the different distribution of the external force applied on the MTs. They think that the conventional simple theory of strength of materials does not hold in this case and that some inhomogeneity of mechanical properties of the MTs is present and play an important role.

By measuring the flexural rigidity, Tuszynski et al. [63] postulated that the shear modulus depends on the magnitude of the deformation whereas Yong's modulus due to longitudinal or lateral forces is only dependent on the structure of MTs. Hence the diversity of experimental data may be explained as arising due to different magnitudes of the forces applied. The gross elastic anisotropic features of MTs are quite well explained by the existing models and parameter values.

Kitumoto et al. [58] made a simple improvement to the buckling force method toward the goal of achieving a reliable estimate even though the reasons for method-dependent discrepancies in the flexural rigidity values are presently unclear. They concluded that there is no length dependency for the flexural rigidity of MTs, length dependency of flexural rigidity is because of different experimental conditions and depth of manipulation. Most of the methods in previous researches assume that the microtubule is a homogeneous and isotropic slender elastic rod, but this assumption is far from true. They suggested that now may be the time to begin regarding the microtubule as a complex structure instead of as a homogeneous isotropic slender elastic rod when conducting experiments to measure flexural rigidity of MTs. Probably complex shell model is a good alternative method for the complex structure of MTs. Based on these analyses, complex shell model has been proposed in measuring and predicting the flexural rigidity of MTs.

Until 2006, Pampaloni et al. [64] systematically studied the dependence of persistence length on the length of MTs. They found this length-dependence of persistence length and interpreted this length-dependence as a consequence of a non-negligible shear deflection determined by sub-nanometer relative displacement of adjacent protofilaments. Because individual microtubule is a tubular assembly of discrete protofilaments assembled in parallel, its mechanical response can be understood by

analogy with anisotropic fiber reinforced materials rather than by a direct application of the theory of elasticity for homogeneous structures. This property can be explained by the anisotropic structure of MTs and described by linear elasticity theory. It is interesting to speculate about the biological significant of this property. MTs are able to accomplish various tasks in differently sizes cells and during different stages of a cell's life cycle.

The above explanations discussed the spreading of estimated flexural rigidity in a large range. We can see that researchers all mentioned the length of the microtubule, but did not explain the length-dependence of flexural rigidity of the MTs which remains in previous works.

1.3 Plan of the thesis

In this section, we will introduce the main objectives of the research and the outline of the thesis, as well as the contributions of this work.

1.3.1 The main objectives of the research

We have two objectives in this thesis. In the following we will introduce them respectively. First, a novel thin-walled elastic beam model has been developed. Taking advantage of this beam model, the present work based on Li et al. [65] is devoted to study critical condition under which uniform bending of a flagellum will cause lateral/torsional buckling of the central pair. The objective of this research is to analyze the critical values and the wavelengths for the lateral buckling of the central pair, to explore the reasons underlying the rotation of central pair, and to provide new insight into the relationship between the torsion of the central pair and the bending of flagella. Second, an orthotropic shell model has been developed for explaining the length-dependence of the flexural rigidity of MTs. Taking advantage of this orthotropic shell model, the present work based on Li et al. [66] is devoted to interpret the unexplained length-dependence of flexural rigidity and Young's modulus of MTs in the previous literatures. The objective of this research is to catch the unique feature of mechanical properties of MTs by predicting the buckling loads and vibration frequencies, to explore the reasons underlying length

dependence of flexural rigidity, and to provide a reasonable explanation for the length dependence of flexural rigidity of MTs by using this orthotropic shell model.

1.3.2 The outline of the thesis

As reviewed above, the mechanics of MTs have been studied extensively in recent years. Some special issues, such as the rotation of the central pair during flagella bending and the scattered values of flexural rigidity of MTs have also been discussed in detail. However, comprehensive study on (1) the rotation of the central pair during flagella bending, (2) length-dependence of flexural rigidity of MTs is still necessary because clear explanation on the above two issues has not been reported and controversy remain in literature. This is because major challenges exist in experiments on small-size MTs, which cannot be readily observed and analyzed without theoretical guidance. Additionally, due to anisotropy of microtubules, the isotropic beam model or classical shell model, in general, cannot obtain satisfactory results when they are directly employed to characterize mechanical property of MTs. On the other hand, the accurate orthotropic shell model for explaining the length-dependence of the flexural rigidity of MTs has been developed, and the elastic beam model on elastic foundation for the torsion of the central pair under bending also has been established. Particularly, the present beam model and orthotropic shell model has been compared to the available experiments to demonstrate its effectiveness.

In what follows, the detailed theoretical derivation and numerical calculations are given for lateral/torsional buckling of the central pair bent in the plane of maximum bending rigidity and in the plane of minimum bending rigidity, and a novel thin-walled elastic beam model is applied into this research problem. Meanwhile, for explaining length-dependence of flexural rigidity of MTs, an orthotropic shell model is suggested to study static buckling and free vibration of MTs and then to compare results with that obtained from isotropic beam model, with existing experimental data and a known formula as well.

In Chapter 2, the general formulations for lateral buckling of the central pair under a uniform bending and for dynamics of an individual microtubule under a uniform axial compressive force are outlined. First, a thin-walled elastic beam model is developed. Two

equilibrium equations are chosen to govern the lateral buckling of the central pair under the uniform bending. Second, to investigate the buckling and free vibration of MTs, three equations are chosen to govern dynamics of an individual microtubule under a uniform axial compressive force. An orthotropic shell model is established based on the above three equations.

In Chapter 3, detailed analysis for lateral buckling of the central pair under uniform bending is discussed. The critical values of bending and the associated wavelengths of buckling mode are calculated. The critical values are found to be sensitive to the parameters defining the surrounding medium, but less sensitive to shear modulus of MTs, the buckling wavelengths are more sensitive to the parameters defining surrounding medium, but less sensitive to the shear modulus when bent in the plane of maximum bending rigidity. In the plane of minimum bending rigidity, although lateral buckling of the central pair is less likely but does occur under critical values.

In Chapter 4, detailed analysis for free vibration of an individual microtubule and buckling of an individual microtubule under compressive force is given. The frequencies and critical buckling loads are predicted by the accurate orthotropic shell model and compared with that given by the approximate isotropic beam model. And also, a critical length of MTs based on free vibration analysis is determined, simultaneously, a critical length of MTs based on buckling analysis is determined. It is shown that vibration frequencies and buckling loads predicted by the accurate orthotropic shell model are much lower than that given by the approximate isotropic beam model for shorter MTs, although the two models give almost identical results for sufficiently long MTs. The length-dependence of flexural rigidity predicted by the orthotropic shell model is compared with that given by existing experimental data and formula. The length-dependence of flexural rigidity predicted by the orthotropic shell model is different from that given by the formula but is in good agreement with that given by existing experimental data. These results confirm that longitudinal Young's modulus of MTs is length-independent, and the observed length-dependence of the flexural rigidity and Young's modulus is a result of strongly anisotropic elastic properties of MTs which have a length-dependent weakening effect on flexural rigidity of shorter MTs.

Finally, in Chapter 5, our conclusions on our two research problems and comments on the models we applied in this thesis are given. The results show that the thin-walled beam model for exploring the torsion of the central pair and the orthotropic shell model for explaining the length-dependence of flexural rigidity of MTs are all in good agreement with published experimental data. Furthermore, we will propose our future plans.

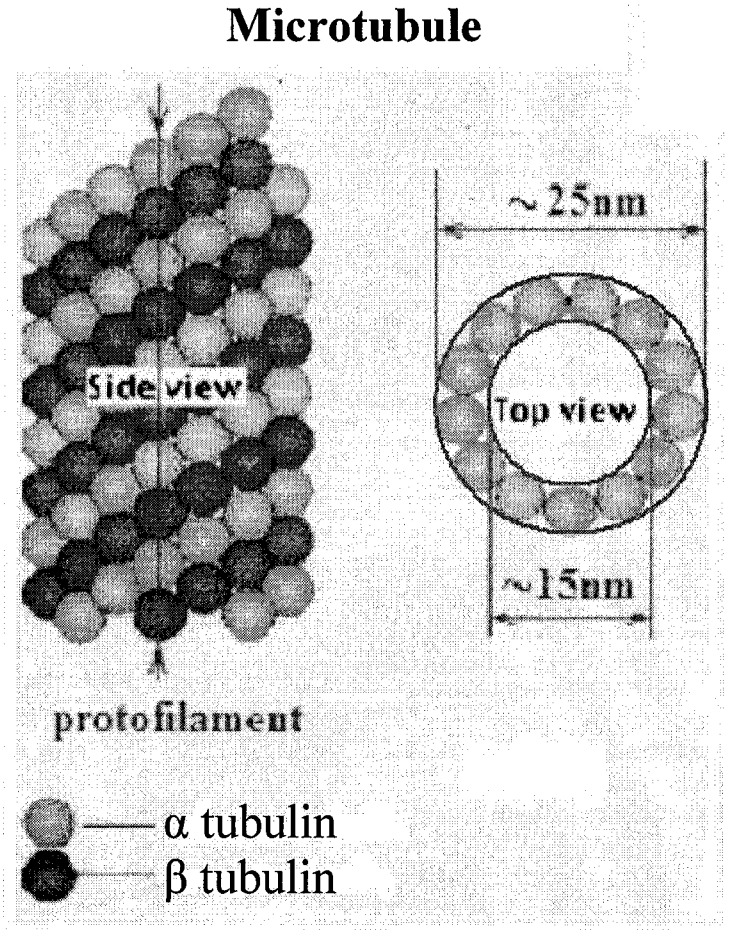

Fig. 1.1 The structure of the MTs

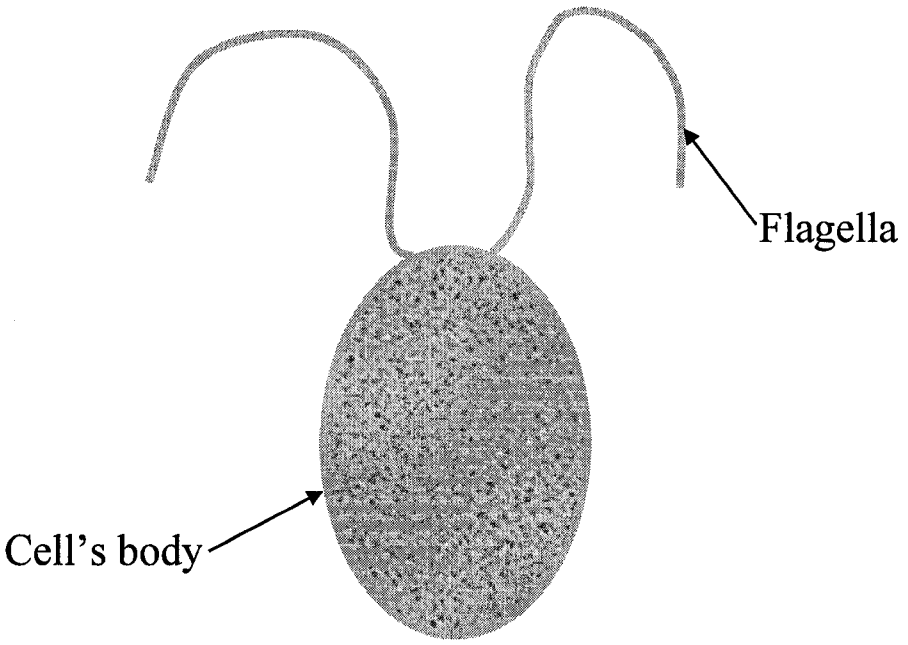

Fig. 1.2 Flagella are long whip-like organelles extending from the cell's body [18].

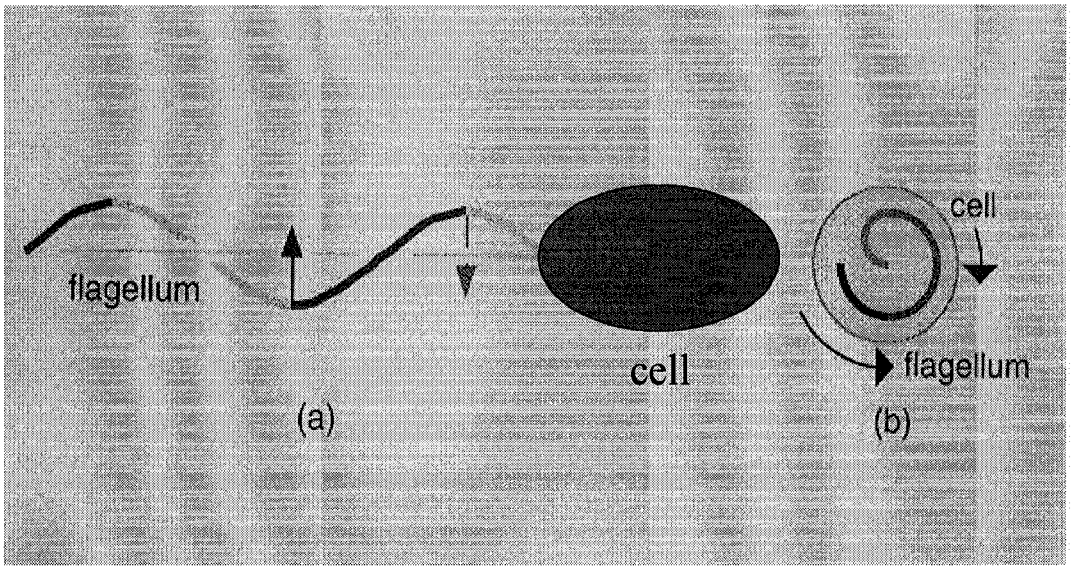

Fig. 1.3 Torque and thrust generated by flagella can move a cell (a) some cells bend their flagella to produce a wavelike motion (b) the flagellum rotates counter-clockwise to provide thrust, and the cell slowly rotates clockwise in response [10].

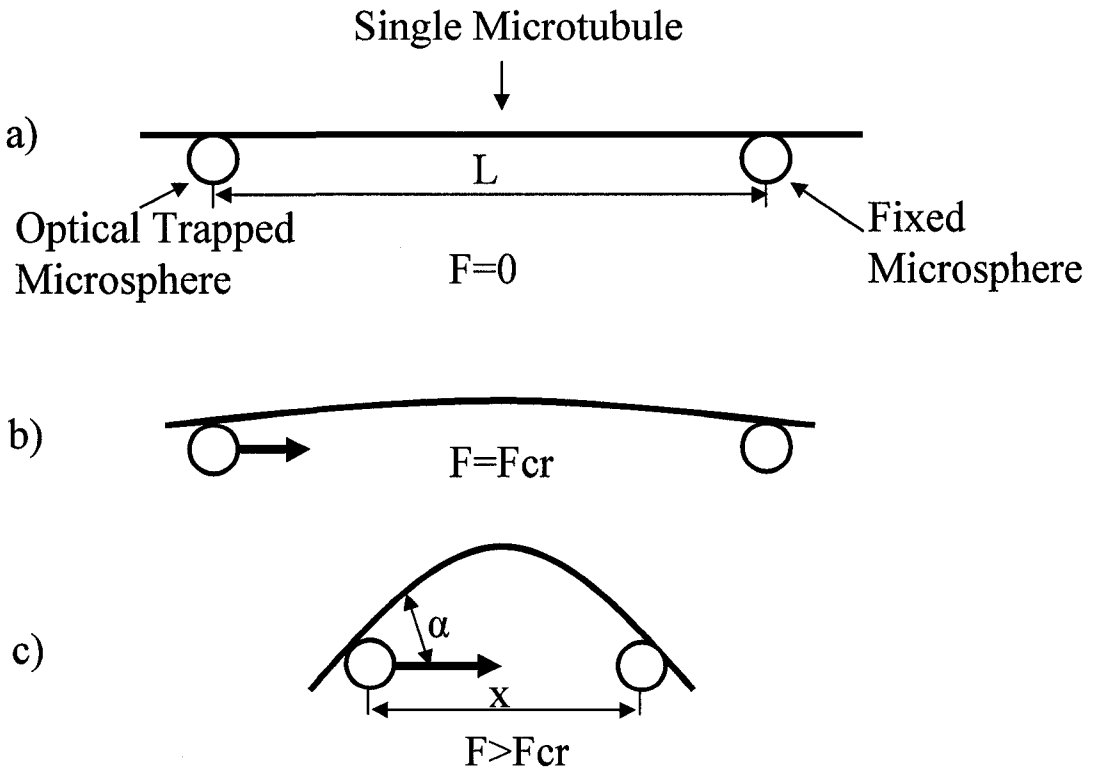

Fig. 1.4 Microtubule modeled as an elastic rod/beam (1) [28] a). The MT is straight when no force is applied, b). The MT is in unstable equilibrium and starts to buckle when F=Fcr, c). The MT is buckling until the limit to balance with the recovery force of MT when F>Fcr.

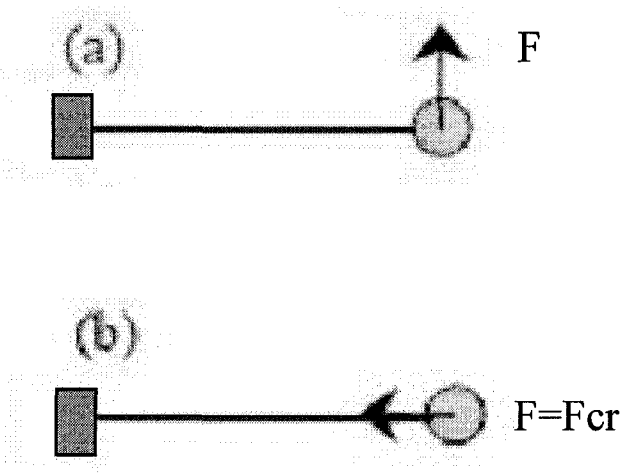

Fig. 1.5 Microtubule modeled as an elastic rod/beam (2) [29] (a) Mode of Bending Deformation, Flexural rigidity: $EI = \frac{FL^3}{3d}$ Where d is the end deflection, L is the length of the microtubule (b) Mode of Compression Deformation, Flexural rigidity: $EI = \frac{F_{cr}L^2}{2.05\pi^2}$

Chapter 2

Elastic Beam and Shell Models Applied in the Research

In scientific research, there are many methods applied. Among a great deal of methods, many studies showed that elastic beam model and elastic shell model have been successfully applied in studying mechanical behaviour of objects subjected to all kinds of loads. Especially in recent years, mechanical behaviours of biological structures at the micro/nano scale have been studied using mechanical models for cell mechanics. In this thesis, we will develop a thin-wall beam model and an orthotropic shell model. We will separately introduce in detail the application of the beam model in studying lateral torsion buckling of the central pair MTs under bending and the shell model in studying the length-dependence of flexural rigidity of MTs.

2.1 The beam model used for torsion of the central pair MTs

Inspired by the structural characteristics of the central pair MTs, and the similarity between bending-related torsion of the central pair MTs and the lateral/torsional buckling of thin-walled elastic beams under bending [67-70], we developed a thin-wall beam model to study whether or not a moderate bending of a flagellum could cause lateral/torsional buckling of the central pair MTs. This subject is motivated especially by the fact that the central pair, as modeled as a single elastic beam, has a lower torsional rigidity. As will be seen from Chapter 3, for the first time in the literature, the thin-wall beam model provides an insight into torsion of the central pair under bending.

In this thesis, we shall focus on structural behavior of the central pair itself, and the effects of all surrounding links and organelles inside the flagellum will be modeled approximately by an equivalent surrounding elastic medium. In this section, this beam model, basic parameters of the central pair and the surrounding elastic medium and governing equations will be discussed.

2.1.1 The model of an elastic beam on elastic foundation

In certain applications, an elastic beam is placed on an elastic foundation and loads are applied to the beam. The loads are transferred through the beam to the foundation. Furthermore, we assume that the foundation resists the force transmitted by the beam in a linearly elastic manner, that is, the pressure developed at any point between the beam and the foundation is proportional to the deflection of the beam at that point. This assumption is fairly accurate for small deflections. Based on above assumptions, the basic equation governing an elastic beam on an elastic foundation is:

$$EI\frac{d^4w(x)}{dx^4}+K\cdot w(x)=0 \tag{2.1}$$

where the spring constant K, defined by the reaction force (per unit axial length of the beam) against the deflection of the beam, E is the longitudinal elastic modulus of the beam, $w(x)$ is the deflection of the beam, EI represents the bending rigidity of the beam.

For large deflections, the stiffness of the foundation could be related in a nonlinear way to the beam deflection. But, here we only consider small deflection to simplify our analysis.

2.1.2 Basic parameters of the central pair and the surrounding elastic medium

The central pair of flagella is composed of two complete single MTs, as shown in Fig. 2.1, surrounded by associated links and organelles. The present study focuses on structural behavior of the central pair itself, and the effects of all surrounding links and organelles inside the flagellum will be modeled approximately by an equivalent surrounding elastic medium, defined by two spring constants for transverse deflections of the central pair and one spring constant for torsion of the cross-section of the central pair.

As a whole, the central pair of MTs, including the bridge linking the two MTs, will be described as a single elastic beam of thin-walled cross-section. Assume that the two MTs of the central pair are initially parallel to each other. Thus, the coordinate system is centered at the centroid of the central pair's cross-section, as shown in Fig. 2.2, where the x-axis is along the axial direction of the flagellum, and the y- and z- axes are along two mutually perpendicular principal directions of the cross-section, of maximum and minimum bending rigidities, respectively.

Let us now calculate bending rigidities EI_{yy} and EI_{zz} ($I_{yz}=0$ due to the symmetry of the cross-section), where E is the longitudinal elastic modulus of MTs of $1\sim2GPa$ [3, 8, 29, 55, 62, 66]. Following the literature, the cross-section of a single microtubule will be treated as an equivalent circular annular shape, with an equivalent thickness $h\approx 3\,nm$ (see e.g. [3, 62]). Thus, all moments of inertia of the cross-section are defined based on such a thickness $h\approx 3\,nm$. In addition, because the bridging linking the two MTs has a much lower elastic modulus than the longitudinal modulus E, the contribution of the bridging to bending rigidities can be neglected. Thus, $EI_{zz}=2E\dfrac{\pi\left(R_o^4-R_i^4\right)}{4}\approx 5.60\times10^{-23}\ N\cdot m^2$, where we have assumed that the medium radius r_m of a single microtubule is $11.5nm$, and the outer radius $R_0=13\,nm$ while the inner radius $R_i=10\,nm$. Similarly, because the distance between the centers of the two MTs is $2a\approx 34nm$ [26] (see Fig. 2.2), the bending rigidity EI_{yy} is obtained by the parallel-axis formula, which gives $EI_{yy}=2E\left[\dfrac{\pi\left(R_o^4-R_i^4\right)}{4}+\pi\left(R_o^2-R_i^2\right)a^2\right]\approx 3.0\times10^{-22}\ N\cdot m^2$.

On the other hand, torsional rigidity of the central pair, GJ, is proportional to shear modulus G of MTs [71, 72]. Because shear modulus G is more than two orders of magnitude lower than the longitudinal Young's modulus E, it is expected that MTs and the central pair have lower torsional rigidities. In particular, the actual value of G is unknown in the literature. Here, following [61, 63], we assume that G is about $10^4\sim10^6$ Pa or $G/E=10^{-5}\sim10^{-3}$. Thus neglecting the contribution of the bridging to torsional rigidity, torsional rigidity of the central pair will be given roughly by twice the torsional rigidity of a single microtubule. Thus, $GJ=2GJ_o=2G\dfrac{\pi\left(R_o^4-R_i^4\right)}{2}$, where G is the shear modulus of MTs [71, 72] and J_o is the torsional constant of a single microtubule. Thus, taking $E=1.9\ GPa$ [63], the values of EI_{yy} and EI_{zz}, and the range of the torsional rigidity GJ are given in Table 2.1.

The central pair is surrounded by mixed cytoplasm fluid and flagellar links. The modulus of cytoplasm fluid is around $10^2\sim10^5$ Pa [73], while the moduli of flagellar links

are around 10^4~$10^6 Pa$ [8]. Therefore, the equivalent modulus E_0 of the surrounding elastic medium can be bounded reasonably by $10^3 < E_0 < 10^6$ Pa. Furthermore, because the ratio of the wavelength to the diameter of the central pair is definitely between 1 and 500, it is verified (see figure 1 of [74] and eqn. (10) of [75]) that the spring constant K_y, defined by the reaction force (per unit axial length of the central pair) against the deflection of the central pair in the y-direction, can be estimated by $K_y = (10^{-2}\sim 1) E_0$. In addition, the spring constant K_y can be assumed to be approximately twice K_z, then $K_z = 0.5 K_y$. Finally, because the distance between the centers of the two MTs is about $2a = 34\, nm$, simple calculation shows that the spring constant K_ϕ, defined by the reaction moment against the rotation of the central pair, can be given approximately by $K_\phi = 2K_y a^2$. The values of all these parameters, used in this thesis for the surrounding elastic medium, are summarized in Table 2.1.

2.1.3 Governing equations

We will discuss the governing equations for lateral buckling of the central pair bent in the plane of maximum bending rigidity and in the plane of minimum bending rigidity, respectively. Critical value of bending will be discussed as well in the following.

2.1.3.1 Governing equations for lateral buckling of the central pair bent in the plane of maximum bending rigidity

First, let us consider torsional/lateral buckling of the central pair when the flagellum is uniformly bent in the x-z plane. Under such a uniform bending, the pre-buckling deflection of the central pair, $w_0(x)$, is a quadratic function of x and thus $EI_{yy} w_0''(x)$ is a constant equal to the moment M_{yy} acting on the central pair prior to buckling ($M_{yy} = EI_{yy} w_0''(x)$). Let that y-directional buckling deflection of the central pair be $v(x)$, and buckling torsion of the cross-section of the central pair about the x-axis be $\phi(x)$. Thus, the reaction force and torque, acting on the central pair due to the

surroundings, are $K_y v(x)$ and $K_\phi \phi(x)$, respectively, and lateral buckling of the central pair under the uniform bending M_{yy} is governed by [67-70]

$$EI_{zz}\frac{d^4 v(x)}{dx^4} - M_{yy}\frac{d^2\phi(x)}{dx^2} + K_y v(x) = 0 \tag{2.2}$$

$$-GJ\frac{d^2\phi(x)}{dx^2} - M_{yy}\frac{d^2 v(x)}{dx^2} + K_\phi \phi(x) = 0 \tag{2.3}$$

Assume that the central pair is hinged at its two ends and thus

$$v(x) = A\sin\frac{m\pi x}{L}, \phi(x) = B\sin\frac{m\pi x}{L} \tag{2.4}$$

where L is the length of the flagellum, A and B are two real numbers, and integer m is the half-wave number of buckling mode. Thus, substituting (2.4) into (2.2, 2.3) gives

$$A\left[EI_{zz}\left(\frac{m\pi}{L}\right)^4 + K_y\right] = M_{yy}(-B)\left(\frac{m\pi}{L}\right)^2 \tag{2.5}$$

$$B\left[GJ\left(\frac{m\pi}{L}\right)^2 + K_\phi\right] = M_{yy}(-A)\left(\frac{m\pi}{L}\right)^2 \tag{2.6}$$

The condition for existence of a non-zero- solution (A , B) gives

$$\left[GJ\left(\frac{m\pi}{L}\right)^2 + K_\phi\right]\left[EI_{zz}\left(\frac{m\pi}{L}\right)^4 + K_y\right] = M_{yy}^2\left(\frac{m\pi}{L}\right)^4 \tag{2.7}$$

The critical value of M_{yy}, for lateral buckling of the central pair, is determined by the lowest M_{yy} with respect to the integer m, and the buckling mode is determined by the associated integer m^*, at which the lowest M_{yy} is obtained, and the associated ratio A/B.

In particular, if the surrounding elastic medium is absent and then $K_y = 0$ and $K_\phi = 0$, the lowest value of M_{yy} is $\frac{\pi}{L}\sqrt{GJEI_{zz}}$ with m^*=1 [67].

2.1.3.2 Governing equations for lateral buckling of the central pair bent in the plane of minimum bending rigidity

It is known that lateral buckling is more likely to occur when a thin-walled beam is bent in the plane of maximum bending rigidity [67, 68], less likely when bent in the plane of minimum bending rigidity. In spite of this, for the sake of completeness, we also consider possible torsional/lateral buckling of the central pair when the flagellum is uniformly bent in the x-y plane of minimum bending rigidity. It is expected that the central pair may also buckle when the bending exceeds a critical value, although the critical value will be much higher than that obtained in the case when the flagellum is uniformly bent in the x-z plane.

Under a uniform bending of the flagellum in the x-y plane, the pre-buckling deflection of the central pair, $v_0(x)$, is a quadratic function of x and thus $EI_{zz}v_0''(x)$ is a constant equal to the moment $M_{zz} = EI_{zz}v_0''(x)$ acting on the central pair prior to buckling. Let that the z-directional buckling deflection of the central pair be $w(x)$, and buckling torsion of the cross-section about the x-axis be $\phi(x)$. Thus, the reaction force and torque, acting on the central pair due to the surroundings, are $K_z w(x)$ and $K_\phi \phi(x)$, respectively, and lateral buckling of the central pair under the uniform bending M_{zz} is governed by [67-70]

$$EI_{yy}\frac{d^4w(x)}{dx^4} + M_{zz}\frac{d^2\phi(x)}{dx^2} + K_z w(x) = 0 \tag{2.8}$$

$$-GJ\frac{d^2\phi(x)}{dx^2} + M_{zz}\frac{d^2w(x)}{dx^2} + K_\phi \phi(x) = 0 \tag{2.9}$$

Assume that the central pair is hinged at its two ends and thus

$$w(x) = C\sin\frac{n\pi x}{L}, \phi(x) = D\sin\frac{n\pi x}{L} \tag{2.10}$$

where C and D are two real numbers, and integer n is the half-wave number of buckling mode. Thus, similar to Section 2.1.3.1, substituting (2.10) into (2.8, 2.9) leads to a condition for existence of a non-zero- solution (C, D) as

$$\left[GJ\left(\frac{n\pi}{L}\right)^2 + K_\phi\right]\left[EI_{yy}\left(\frac{n\pi}{L}\right)^4 + K_z\right] = M_{zz}^2\left(\frac{n\pi}{L}\right)^4 \tag{2.11}$$

The critical value of M_{zz}, for lateral buckling of the central pair, is determined by the lowest M_{zz} with respect to the integer n, and the buckling mode is determined by the associated integer n^*, at which the lowest M_{zz} is obtained, and the associated ratio *C/D*.

2.2 The orthotropic shell model used for MTs

In this thesis, an orthotropic shell model has been applied to study vibration frequencies and buckling loads of MTs. A detailed description will be given about the orthotropic shell model, material constants and bending stiffness, and governing equations in the following.

2.2.1 The orthotropic elastic shell model

The study of free vibration behaviour of isotropic cylindrical shells has been carried out by many investigators. Most of their works were developed originally for thin elastic shells, in both linear and nonlinear cases. They are based on the classical shell theory, which could lead to gross error in the prediction of transverse deflections, natural frequencies and buckling loads of anisotropic shell or moderately thick shell due to the neglect of transverse shear deformations. In the light of these problems, a number of theories for anisotropic shell exist in literature. The current orthotropic elastic shell model is developed on the basis of the theories for MTs as anisotropic shell.

MTs have a hollow cylindrical shell-like shape constructed of typically 13 parallel protofilaments aligned longitudinally [7-10]. Recent experiments have shown that the longitudinal bonds between tubulin dimers along protofilaments are much stronger than the lateral bonds between adjacent protofilaments [76-78]. In particular, shear modulus of MTs is much lower than elastic modulus along longitudinal direction, and circumferential elastic modulus is lower than longitudinal elastic modulus by a few orders of magnitude [4, 61, 63]. As an elastic rod or beam, the flexural rigidity of a MT is expressed by ($E_x I$), where E_x is the longitudinal Young's modulus and I is the moment of inertia of the cross-section. Obviously, the flexural rigidity depends only on the longitudinal Young's modulus, and not on the much lower shear modulus and circumferential modulus. Since the longitudinal modulus becomes dominant only for very long MTs, it is anticipated that much lower shear modulus and circumferential Young's modulus would weaken flexural rigidity of shorter MTs, and are likely responsible for the observed length-dependence of the flexural rigidity of MTs. Motivated by this idea, an orthotropic shell model is used to examine this issue.

2.2.2 Four independent material constants

Here, a microtubule is modeled as an orthotropic elastic shell longitudinally reinforced by protofilaments (as "fiber") (see Fig. 2.3). It is known that an orthotropic shell has four independent material constants, including longitudinal modulus E_x, circumferential modulus E_θ, shear modulus $G_{x\theta}$, and Poisson ratio ν_x along longitudinal direction [79, 80] (ν_θ, the Poisson ratio in circumferential direction, is determined by the relation $\frac{\nu_\theta}{\nu_x} = \frac{E_\theta}{E_x}$). The values of the longitudinal modulus E_x, circumferential modulus E_θ and Poisson ratio ν_x of MTs can be identified from the data available in the literature [3, 4, 61-63] and shown in Table 2.2.

On the other hand, shear modulus of protofilaments is about 1.4 *MPa* [4, 52-53, 61, 63], while shear modulus between adjacent MTs or protofilaments (called "longitudinal shearing" in [63]) is as low as 1 *KPa* [57, 63]. According to the formula [81, 82] for effective shear modulus of a longitudinally fiber-reinforced orthotropic

elastic shell, the shear modulus $G_{x\theta}$ of orthotropic shell can be estimated by $1/G_{x\theta} = V_f/G_f + V_m/G_m$, where V_f and V_m are volume fractions of the fiber and matrix phases, and G_f and G_m are shear moduli of the fiber and matrix. For MTs longitudinally reinforced by protofilaments, volume of protofilaments is dominant and then V_m/V_f should be much smaller than unity. For example, using G_f=1 *MPa* and G_m=1 *KPa* as suggested above, the shear modulus of MTs is estimated to be about 10 *KPa* for V_m/V_f=0.1, or 0.1 *MPa* for V_m/V_f=0.01. Here, it is noticed that shear modulus for MTs suggested in [63], based on a rough estimate, ranges from 0.05 *KPa* to 0.5 *MPa*. Therefore, according to all of these available data, it is reasonable to assume that (effective) shear modulus of MTs, as an orthotropic elastic shell, should be much lower than 1 *MPa*. For example, it seems reasonable to assume that the shear modulus of MTs ranges between 10 *KPa* and 0.1 *MPa*, as shown in Table 2.2.

According to the literature, the circular cross-section of MTs will be treated as an equivalent circular annular shape, with an equivalent thickness $h \approx 2.7nm$ (see e.g. [3, 62]). Thus, all elastic moduli and in-plane stiffnesses, as well as the mass density ρ, are defined based on such a thickness $h = 2.7nm$. For example, three in-plane stiffnesses, K_x, K_θ and $K_{x\theta}$, are defined as

$$K_x = \frac{E_x h}{1-\nu_x \nu_\theta},\ K_\theta = \frac{E_\theta h}{1-\nu_x \nu_\theta},\ K_{x\theta} = G_{x\theta} h \tag{2.12}$$

where h=2.7*nm*. On the other hand, because of discrete lattice structure of MTs, the bending stiffness of MTs is largely determined by a so-called "bridge" thickness of MTs (about 1.1*nm*, see figure 2 of [62] or Fig. 2.3) which is much smaller than the thickness h=2.7*nm*. Thus, similar as single-walled carbon nanotubes [75, 83], the effective bending stiffness of MTs is considered as an independent material constant. According to experimental data on shell-like buckling of individual microtubule given in [62], the bending stiffness of MTs can be calculated by an effective thickness h_0 =1.6*nm*. Thus, the effective bending stiffness in longitudinal direction D_x, the effective bending stiffness

in circumferential direction D_θ, and effective bending stiffness in shear $D_{x\theta}$, are given by

$$D_x = \frac{E_x h_0^3}{12(1-\nu_x \nu_\theta)},\ D_\theta = \frac{E_\theta h_0^3}{12(1-\nu_x \nu_\theta)},\ D_{x\theta} = \frac{G_{x\theta} h_0^3}{12} \tag{2.13}$$

where $G_{x\theta}$ is the shear modulus of MTs (between $10\,KPa$ and $0.1\,MPa$, as shown in Table 2.2), and h_0 (= $1.6nm$) is the effective thickness for bending.

2.2.3 Governing equations of the orthotropic elastic shell model

Modeled as an orthotropic elastic shell, dynamics of an individual microtubule, under a uniform axial compressive force N_x, is governed by three equations [84-87]

$$\begin{Bmatrix} (1+\frac{N_x}{K_x})\cdot r^2 \cdot \frac{\partial^2}{\partial x^2} + \\ \beta\cdot(1+\gamma)\cdot\frac{\partial^2}{\partial\theta^2} \end{Bmatrix}\cdot u + \left\{(\alpha\nu_x+\beta)\cdot r\cdot\frac{\partial^2}{\partial x\partial\theta}\right\}\cdot v + \begin{Bmatrix} -\alpha\nu_x\cdot r\cdot\frac{\partial}{\partial x} \\ +\gamma\cdot r^3\cdot\frac{\partial^3}{\partial x^3} \\ -\beta\cdot\gamma\cdot r\cdot\frac{\partial^3}{\partial x\partial\theta^2} \end{Bmatrix}\cdot w$$
$$= \left(\frac{r}{S_L}\right)^2 \cdot \frac{\partial^2 u}{\partial t^2},$$

$$\left\{(\alpha\nu_x+\beta)\cdot r\cdot\frac{\partial^2}{\partial x\partial\theta}\right\}\cdot u + \begin{Bmatrix} \alpha\cdot\frac{\partial^2}{\partial\theta^2} \\ +\left(\beta\cdot(1+3\gamma)+\frac{N_x}{K_x}\right)\cdot r^2\cdot\frac{\partial^2}{\partial x^2} \end{Bmatrix}\cdot v + \begin{Bmatrix} -\alpha\cdot\frac{\partial}{\partial\theta} \\ +\gamma\cdot(\alpha\nu_x+3\beta)\cdot r^2\cdot\frac{\partial^3}{\partial x^2\partial\theta} \end{Bmatrix}\cdot w$$
$$= \left(\frac{r}{S_L}\right)^2 \cdot \frac{\partial^2 v}{\partial t^2},$$

$$\begin{Bmatrix} \alpha\nu_x \cdot r \cdot \dfrac{\partial}{\partial x} \\ -\gamma \cdot r^3 \cdot \dfrac{\partial^3}{\partial x^3} + \\ +\gamma \cdot \beta \cdot r \cdot \dfrac{\partial^3}{\partial x \partial \theta^2} \end{Bmatrix} \cdot u + \begin{Bmatrix} \alpha \cdot \dfrac{\partial}{\partial \theta} \\ -\gamma \cdot (\alpha\nu_x + 3\beta) \cdot r^2 \cdot \dfrac{\partial^3}{\partial x^2 \partial \theta} \end{Bmatrix} \cdot v + \begin{Bmatrix} -\gamma \cdot r^4 \cdot \dfrac{\partial^4}{\partial x^4} \\ -2\gamma \cdot (\alpha\nu_x + 2\beta) \cdot r^2 \cdot \dfrac{\partial^4}{\partial x^2 \partial \theta^2} \\ -\alpha \cdot \gamma \cdot \left(\dfrac{\partial^2}{\partial \theta^2} + 1 \right)^2 - \alpha \\ + \dfrac{N_x}{K_x} \cdot r^2 \cdot \dfrac{\partial^2}{\partial x^2} \end{Bmatrix} \cdot w$$

$$= \left(\frac{r}{S_L} \right)^2 \cdot \frac{\partial^2 w}{\partial t^2}$$

(2.14)

where x and θ are axial coordinate and circumferential angular coordinate, respectively, u, v and w are axial displacement, circumferential displacement and radial (inward) deflection, respectively, ρ is the mass density (per unit volume), h (=2.7nm) is equivalent thickness of the microtubule, and r is the average radius. In addition, $\alpha = \frac{\nu_\theta}{\nu_x} = \frac{E_\theta}{E_x} = \frac{K_\theta}{K_x} = \frac{D_\theta}{D_x}$ and $\beta = \frac{G_{x\theta}}{E_x} \approx \frac{G_{x\theta}}{E_x}(1 - \alpha\nu_x^2) = \frac{D_{x\theta}}{D_x} = \frac{K_{x\theta}}{K_x}$ ($\alpha \cdot \nu_x^2 \to 0$ see Table 2.2), $\gamma = \frac{h_0^3}{12hr^2}$ and the longitudinal sound speed $S_L = \sqrt{\frac{K_x}{\rho h}} \approx \sqrt{\frac{E_x}{\rho}}$. Thus, for given parameters h and h_0, the orthotropic shell model is characterized by four parameters E_x, ν_x, α and β. In particular, the orthotropic shell model (2.14) reduces to an isotropic shell model if α=1 and $\beta = \frac{(1-\nu_x)}{2}$, as illustrated in [87].

2.2.3.1 Governing equations for free vibration of MTs

Modeled as an orthotropic elastic shell, free vibration of an individual microtubule, is governed by three equations [84-87]

$$\begin{Bmatrix} \cdot r^2 \cdot \dfrac{\partial^2}{\partial x^2} + \\ \beta \cdot (1+\gamma) \cdot \dfrac{\partial^2}{\partial \theta^2} \end{Bmatrix} \cdot u + \left\{ (\alpha \nu_x + \beta) \cdot r \cdot \frac{\partial^2}{\partial x \partial \theta} \right\} \cdot v + \begin{Bmatrix} -\alpha \nu_x \cdot r \cdot \dfrac{\partial}{\partial x} \\ +\gamma \cdot r^3 \cdot \dfrac{\partial^3}{\partial x^3} \\ -\beta \cdot \gamma \cdot r \cdot \dfrac{\partial^3}{\partial x \partial \theta^2} \end{Bmatrix} \cdot w$$

$$= \left(\frac{r}{S_L} \right)^2 \cdot \frac{\partial^2 u}{\partial t^2},$$

$$\left\{ (\alpha \nu_x + \beta) \cdot r \cdot \frac{\partial^2}{\partial x \partial \theta} \right\} \cdot u + \begin{Bmatrix} \alpha \cdot \dfrac{\partial^2}{\partial \theta^2} \\ +\beta \cdot (1+3\gamma) \cdot r^2 \cdot \dfrac{\partial^2}{\partial x^2} \end{Bmatrix} \cdot v + \begin{Bmatrix} -\alpha \cdot \dfrac{\partial}{\partial \theta} \\ +\gamma \cdot (\alpha \nu_x + 3\beta) \cdot r^2 \cdot \dfrac{\partial^3}{\partial x^2 \partial \theta} \end{Bmatrix} \cdot w$$

$$= \left(\frac{r}{S_L} \right)^2 \cdot \frac{\partial^2 v}{\partial t^2},$$

$$\begin{Bmatrix} \alpha \nu_x \cdot r \cdot \dfrac{\partial}{\partial x} \\ -\gamma \cdot r^3 \cdot \dfrac{\partial^3}{\partial x^3} + \\ +\gamma \cdot \beta \cdot r \cdot \dfrac{\partial^3}{\partial x \partial \theta^2} \end{Bmatrix} \cdot u + \begin{Bmatrix} \alpha \cdot \dfrac{\partial}{\partial \theta} \\ -\gamma \cdot (\alpha \nu_x + 3\beta) \cdot r^2 \cdot \dfrac{\partial^3}{\partial x^2 \partial \theta} \end{Bmatrix} \cdot v + \begin{Bmatrix} -\gamma \cdot r^4 \cdot \dfrac{\partial^4}{\partial x^4} \\ -2\gamma \cdot (\alpha \nu_x + 2\beta) \cdot r^2 \cdot \dfrac{\partial^4}{\partial x^2 \partial \theta^2} \\ -\alpha \cdot \gamma \cdot \left(\dfrac{\partial^2}{\partial \theta^2} + 1 \right)^2 - \alpha \end{Bmatrix} \cdot w$$

$$= \left(\frac{r}{S_L} \right)^2 \cdot \frac{\partial^2 w}{\partial t^2} \tag{2.15}$$

where the parameters are equivalent to those of equation (2.14).

2.2.3.2 Governing equations for buckling of MTs

Modeled as an orthotropic elastic shell, axially compression buckling of an individual microtubule, under a uniform axial compressive force N_x, is governed by three equations [84-87]

$$\left\{\begin{array}{l}(1+\frac{N_x}{K_x})\cdot r^2\cdot\frac{\partial^2}{\partial x^2}+\\ \beta\cdot(1+\gamma)\cdot\frac{\partial^2}{\partial\theta^2}\end{array}\right\}\cdot u+\left\{(\alpha\nu_x+\beta)\cdot r\cdot\frac{\partial^2}{\partial x\partial\theta}\right\}\cdot v+\left\{\begin{array}{l}-\alpha\nu_x\cdot r\cdot\frac{\partial}{\partial x}\\ +\gamma\cdot r^3\cdot\frac{\partial^3}{\partial x^3}\\ -\beta\cdot\gamma\cdot r\cdot\frac{\partial^3}{\partial x\partial\theta^2}\end{array}\right\}\cdot w$$

$$=0,$$

$$\left\{(\alpha\nu_x+\beta)\cdot r\cdot\frac{\partial^2}{\partial x\partial\theta}\right\}\cdot u+\left\{\begin{array}{l}\alpha\cdot\frac{\partial^2}{\partial\theta^2}\\ +\left(\beta\cdot(1+3\gamma)+\frac{N_x}{K_x}\right)\cdot r^2\cdot\frac{\partial^2}{\partial x^2}\end{array}\right\}\cdot v+\left\{\begin{array}{l}-\alpha\cdot\frac{\partial}{\partial\theta}\\ +\gamma\cdot(\alpha\nu_x+3\beta)\cdot r^2\cdot\frac{\partial^3}{\partial x^2\partial\theta}\end{array}\right\}\cdot w$$

$$=0,$$

$$\left\{\begin{array}{l}\alpha\nu_x\cdot r\cdot\frac{\partial}{\partial x}\\ -\gamma\cdot r^3\cdot\frac{\partial^3}{\partial x^3}+\\ +\gamma\cdot\beta\cdot r\cdot\frac{\partial^3}{\partial x\partial\theta^2}\end{array}\right\}\cdot u+\left\{\begin{array}{l}\alpha\cdot\frac{\partial}{\partial\theta}\\ -\gamma\cdot(\alpha\nu_x+3\beta)\cdot r^2\cdot\frac{\partial^3}{\partial x^2\partial\theta}\end{array}\right\}\cdot v+\left\{\begin{array}{l}-\gamma\cdot r^4\cdot\frac{\partial^4}{\partial x^4}\\ -2\gamma\cdot(\alpha\nu_x+2\beta)\cdot r^2\cdot\frac{\partial^4}{\partial x^2\partial\theta^2}\\ -\alpha\cdot\gamma\cdot\left(\frac{\partial^2}{\partial\theta^2}+1\right)^2-\alpha\\ +\frac{N_x}{K_x}\cdot r^2\cdot\frac{\partial^2}{\partial x^2}\end{array}\right\}\cdot w$$

$$=0 \tag{2.16}$$

where the parameters are equivalent to those of equation (2.14).

In summary, a thin-wall beam model for investigating the torsion of the central pair under bending and an orthotropic shell model for studying the length dependence of flexural rigidity of MTs have been developed. In Chapter 3, torsion of the central pair under bending will be analyzed by using the beam model developed in this chapter. The length dependence of flexural rigidity will also be analyzed in Chapter 4 by using the orthotropic shell model developed in this chapter.

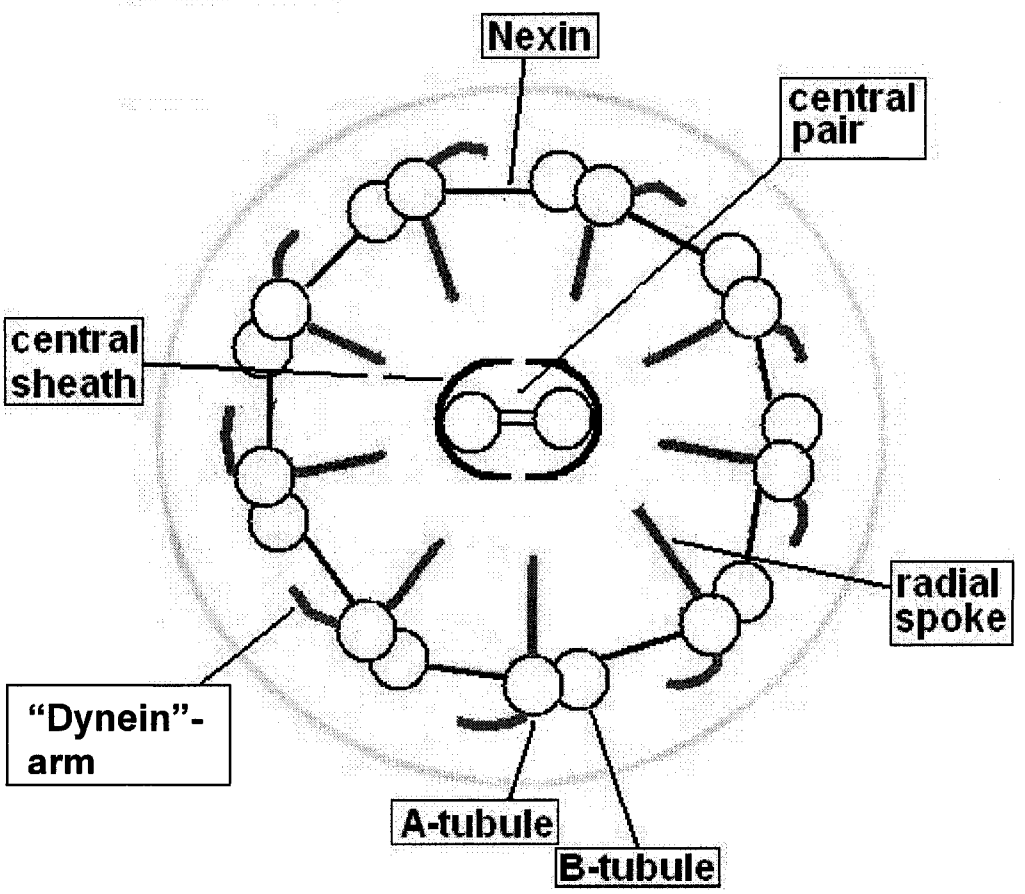

Fig 2.1 The "9+2" axoneme of flagella and cilia.

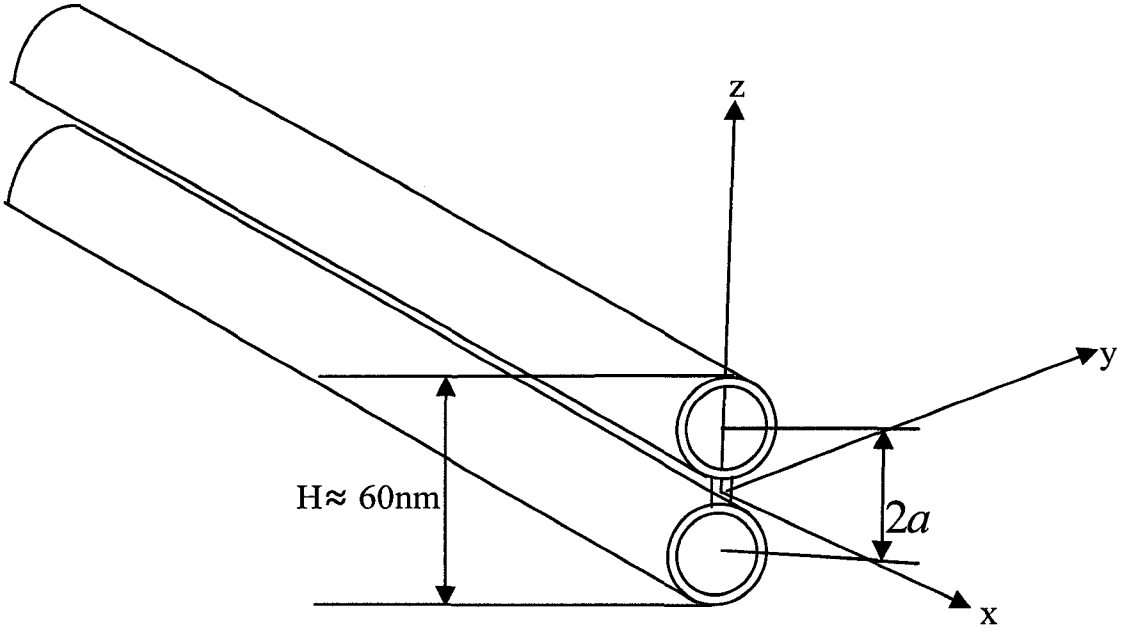

Fig. 2.2 The central pair MTs modeled as a single elastic beam.

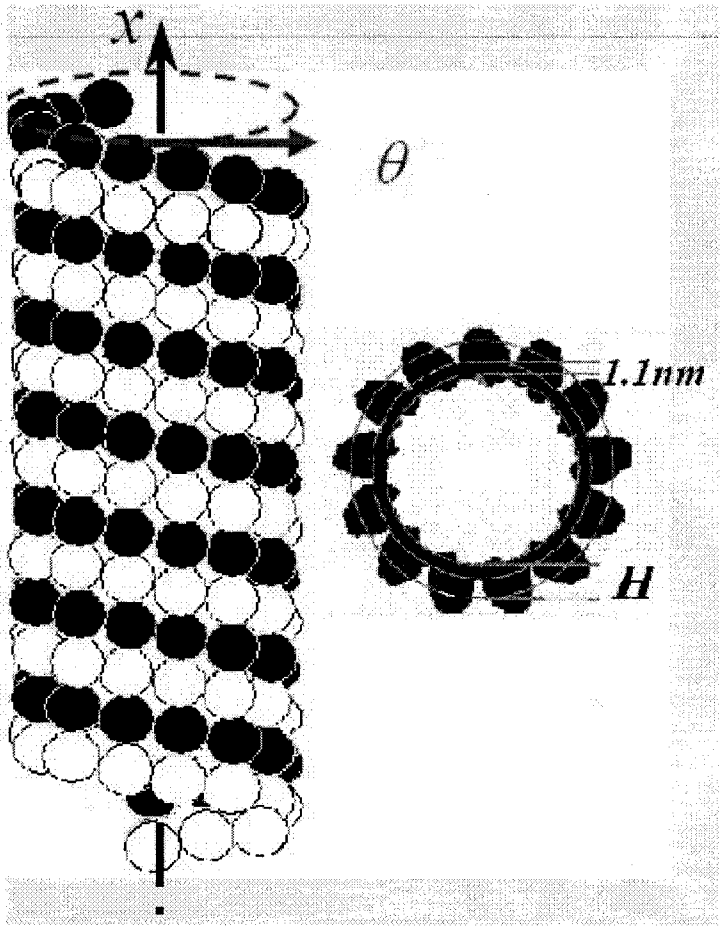

Fig. 2.3 Microtubule modeled as an orthotropic shell model.

Table 2.1 Parameters used in the thesis for the cross-section of the central pair and the equivalent surrounding elastic medium.

Parameters	Value	Reference
r_m	$11.5nm$	[26]
a	$17nm$	[26]
E	$1.9GPa$	[63, 65]
E_0	10^3~$10^6 Pa$	[8, 65, 73]
K_y	$(10^{-2}\sim 1)\,E_0$	[65, 74]
K_z	$0.5\,K_y$	[65]
K_ϕ	$2\,K_y\,a^2$	[65]
G/E	10^{-5}~10^{-3}	[61, 63, 65]
EI_{yy}	$3.00\times10^{-22} N.m^2$	[65]
EI_{zz}	$5.60\times10^{-23} N.m^2$	[65]
GJ	10^{-27}~$10^{-25}\ N.m^2$	[65]
h	$3nm$	[3, 62, 65]
H	$60nm$	[26]

Table 2.2 The values of orthotropic elastic constants for MTs.

Parameters	Values	References
Longitudinal modulus E_x	0.5~2 GPa	[3, 62, 63]
Circumferential modulus E_θ	1~4 MPa	[63]
Shear modulus of protofilaments (lateral shearing [63])	~1 MPa	[52, 62, 63]
(Effective) Shear modulus of MTs $G_{x\theta}$	10 KPa ~ 0.1 MPa	[63]
Poisson's ratio in axial direction ν_x	0.3	[3,63]
Mass density per unit volume ρ	$1.47\,g/cm^3$	[3]
Equivalent thickness h	$2.7nm$	[3, 62]
Effective thickness for bending h_0	$1.6nm$	[62]

Chapter 3

Torsion of the Central Pair MTs in Eukaryotic Flagella due to Bending-driven Lateral Buckling

3.1 Introduction

Cells can move with respect to their environment such as a fluid medium. A common propulsion mechanism for cell movement employs flagella. In spite of a wide variety of eukaryotic cells, eukaryotic flagella consist of a unique common core structure, called "9+2" axoneme, that is about 200*nm* in diameter [9, 10] and contains nine outer doublet MTs, equally spaced in a circle, and two bridged central pair of MTs apart by a small distance of a few nanometers.

Mechanical behavior of flagella, especially rod-like bending deformation of flagella and their hydrodynamic interaction with a surrounding fluid medium, are crucial for their biological functions. It is now widely accepted that bending and motility of flagella are generated by the dynein-driven sliding between doublet MTs [9, 10]. So, sliding-bending mechanics of flagella [12, 26, 30-35], and related hydrodynamics of flagella in a fluid medium [16, 36-42] have been the focus of numerous earlier and recent experimental and theoretical researches.

More recently, a remarkable issue which has attracted considerable attention is bending-related torsion of the central pair MTs of flagella [20, 21, 43-48]. The exact mechanism and functions of torsion of the central pair are not yet fully understood. Since the central pair is believed to play a vital role in regulation of flagella motion [49, 50], it is relevant to study the mechanism responsible for torsion of the central pair MTs in eukaryotic flagella.

Thus, in this chapter, the mechanism responsible for torsion of the central pair MTs in eukaryotic flagella will be studied based on the thin-wall beam model we developed in Chapter 2.

The thin-wall beam model will be used to study whether or not a moderate bending of a flagellum could cause lateral/torsional buckling of the central pair. The justifications and details of the suggested elastic beam model have been given in Chapter 2. The model will be used in Section 3.2 to examine the critical bending and the wavelength of torsional buckling mode when the flagellum is bent in the principal plane of the central pair's cross-section of maximum bending rigidity. Similarly, a flagellum bent in another principal plane of the central pair's cross-section of minimum bending rigidity is studied in Section 3.3. Finally, in Section 3.4, the results and discussion are summarized. As will be seen from Section 3.2, 3.3, and 3.4, for the first time in the literature, the present model shows that torsion of the central pair will occur inevitably, as a result of bending-driven lateral buckling, when a flagellum is bent and the bending exceeds a moderate critical value.

3.2 Lateral buckling of the central pair bent in the plane of maximum bending rigidity

Lateral buckling of the central pair can easily occur when the central pair is bent in the plane of maximum bending rigidity. In this section, we will examine under what critical value lateral buckling of central pair will occur when the central pair is bent in the plane of maximum bending rigidity.

3.2.1 The critical value for lateral buckling of the central pair

The critical value of bending, given in terms of the ratio of the flagellum length to the radius of curvature of the bent flagellum ($Lw_0''(x)$), and the associated buckling mode, given in terms of the ratio of the buckling half-wave length to the height of the central pair, are shown in Fig. 3.1 and Fig. 3.2, respectively, as a function of the length L of the flagellum. Here, it is stated that the (lowest) critical value for lateral buckling is associated with discontinuous mode-number (integer) m when the length L increases. This is responsible for the non-smoothness of the curves given in these figures for smaller flagellum lengths. This phenomenon is common in elastic buckling problems [67, 68].

First, it is seen from Fig. 3.1 that for sufficiently long flagella (say, $L>50H=3\mu m$, where H is the height of the central pair, as shown in Fig. 2.2 and Table 2.1), the critical

value of the ratio ($\frac{M_{yy}L}{EI_{yy}}$) is directly proportional to L/H, which implies that the critical value of the moment M_{yy}, or the critical value of the radius of curvature of the bent flagellum $w_0''(x)=\frac{M_{yy}}{EI_{yy}}$, is independent of the length L. It should be stated that this conclusion essentially lies on the presence of the surrounding elastic medium. In fact, as stated above, in the absence of the surrounding elastic medium (K_y=0 and K_ϕ=0), the critical value of M_{yy} for lateral buckling is inversely proportional to the length L. This can also be seen from the curve for $E_0=10^3$ Pa in Fig. 3.1a), where the surround medium is extremely weak and, as a result, the critical value of ($\frac{M_{yy}L}{EI_{yy}}$) is almost independent of the length L within the range L/H<50.

Another conclusion drawn from Fig. 3.1 is that the critical value for lateral buckling of the central pair is sensitive to the parameters defining the surrounding medium, but less sensitive to the shear modulus G of MTs. Indeed, comparing Fig. 3.1a) and b) with Fig. 3.1c) and d) indicates that an increase of shear modulus G from $10^{-5}E$ to $10^{-3}E$ does not substantially change the critical value for lateral buckling. For example, for $E_0=10^5$ Pa and $K_y=0.01E_0$, it is seen from Fig. 3.1a) and c) that the critical radius of curvature is 50μm for $G=10^{-5}E$, and 30μm for $G=10^{-3}E$. For $E_0=10^4$ Pa and $K_y=E_0$, it is seen from Fig. 3.1b) and d) that the critical radius of curvature is 15μm for $G=10^{-5}E$, and 12μm for $G=10^{-3}E$.

3.2.2 The buckling wavelength of the central pair

As one major conclusion for the buckling wavelength, it is seen from Fig. 3.2 that for sufficiently long flagella (say, L >200H=12μm), the wavelength of the buckling mode is insensitive to the length L. It should be stressed that this conclusion essentially lies on the presence of the surrounding elastic medium. In fact, as stated above, in the absence of the surrounding elastic medium (K_y=0 and K_ϕ=0), the half-wave number m^*=1, and thus the half-wavelength of the buckling mode is equal to the flagellum

length L. This can also be seen from the curve for $E_0=10^3\ Pa$ in Fig. 3.2a), where the surround medium is extremely weak and, as a result, the half-wavelength $L/(m^*H)$ linearly increases with the length L within the range $L/H<100$.

The wavelength of buckling mode for sufficiently long flagella can be estimated from Fig. 3.2. In particular, the buckling wavelength is sensitive to the parameters defining the surrounding medium, but less sensitive to the shear modulus G of MTs. For example, when $E_0=10^3\ Pa$ and $K_y=E_0$, it is seen from Fig. 3.2b) and d) that the buckling wavelength is $1.2\mu m$ for $G=10^{-5}E$, and $2.4\mu m$ for $G=10^{-3}E$. On the other hand, for $E_0=10^4\ Pa$ and $K_y=0.01\ E_0$, it is seen from Fig. 3.2a) and c) that the wavelength is $2.4\mu m$ for $G=10^{-5}E$, and $4.8\mu m$ for $G=10^{-3}E$. We noticed that these predicted wave-lengths are comparable to related wavelengths ($7\sim10\mu m$) observed previously [20-21, 43-48].

Table 3.1 illustrates the critical radius of curvature and buckling wavelength in the case when the central pair is bent in the plane of maximum rigidity.

3.3 Lateral buckling of the central pair bent in the plane of minimum bending rigidity

In this section, we will examine under what critical value lateral buckling of the central pair will occur when the central pair is bent in the plane of minimum bending rigidity. Theoretically, lateral buckling of the central pair only has a little chance to occur when central pair bent in the plane of minimum bending rigidity. However, it could occur when the central pair is bent so severely that the radius of curvature decreases to only few microns.

3.3.1 The critical value for lateral buckling of the central pair

The critical value of bending, given in terms of the ratio of the flagellum length to the radius of curvature of the bent flagellum ($Lv_0''(x)$), and the associated buckling mode, given in terms of the ratio of the buckling half-wave length to the height of the central pair, are shown in Fig. 3.3 and Fig. 3.4, respectively, as a function of the length L of the flagellum. First of all, comparing Fig. 3.3 with Fig. 3.1 indicates that the critical

curvature of the flagellum bent in the x-y plane is one order of magnitude higher than the critical curvature of the flagellum bent in the x-z plane discussed in Section 3.2. This implies that lateral/torsional buckling of the central pair is much more unlikely when the flagellum is bent in the x-y plane of minimum bending rigidity. For example, for $E_0=10^5$ Pa and $K_y=0.01\,E_0$, it is seen from Fig. 3.3a) and c) that the critical radius of curvature of the bent flagellum is $4\mu m$ for $G=10^{-5}E$, and $3\mu m$ for $G=10^{-3}E$. On the other hand, for $E_0=10^3$ Pa and $K_y=E_0$, it is seen from Fig. 3.3b) and d) that the critical radius of curvature is $4\mu m$ for $G=10^{-5}E$, and $3\mu m$ for $G=10^{-3}E$. Therefore, lateral/torsional buckling of the central pair bent in the x-y plane could occur only when it is bent so severely that the radius of curvature downs to only few microns.

3.3.2 The buckling wavelength of the central pair

In case lateral buckling of the central pair bent in the x-y plane occurs, it is seen from Fig. 3.4 that the associated buckling wavelengths are relatively larger than those discussed in Section 3.2 for flagella bent in the x-z plane. Furthermore, it is seen from Fig. 3.4 that the wavelengths of the buckling mode are also insensitive to the length L for sufficiently long flagella (say, $L>300H=18\mu m$). For example, for $E_0=10^3$ Pa and $K_y=E_0$, it is seen from Fig. 3.4b) and d) that the buckling wavelength is $1.8\mu m$ for $G=10^{-5}E$, and $4\mu m$ for $G=10^{-3}E$. On the other hand, for $E_0=10^4$ Pa and $K_y=0.01\,E_0$, it is seen from Fig. 3.4a) and c) that the wavelength is $4\mu m$ for $G=10^{-5}E$, and $9\mu m$ for $G=10^{-3}E$. These data are also comparable to related wavelengths ($7\sim10\mu m$) observed previously [20-21, 43-48].

Table 3.2 illustrates the critical radius of curvature and buckling wavelength in the case when the central pair is bent in the plane of maximum rigidity.

3.4 Summary and discussion

In summary, a thin-walled elastic beam model was suggested to study why the central pair of eukaryotic flagella twists under bending. The results show that torsion of the central pair will occur inevitably, as a result of bending-driven lateral buckling of the central pair, especially when the flagellum is bent in the plane of the central pair's

cross-section of maximum bending rigidity. In this case, the critical curvature of bent flagellum for torsional buckling of the central pair is reasonably small and falls within a range of practical significance for flagellar motility. In particular, for a wide range of estimated parameters, the wave-lengths of the buckling mode predicted by the present model are about a few microns and comparable to some known related data. It is believed that the present model identities an important driving force for bending-related torsion of the central pair, which has apparently not been uncovered in all previous related researches.

Here, it should be stated that the present model is subjected to several limitations. First, the buckling analysis conducted here is limited to static pure bending, although actual bending of flagella is always dynamic in nature and characterized by time-dependent and spacially non-uniform bending moment. Next, the present analysis is restricted to linearized small deflections of the flagellum and small rotations of the central pair. The dynamic and geometrically nonlinear effects on bending-driven torsional buckling of the central pair constitute a few interesting topics for further research.

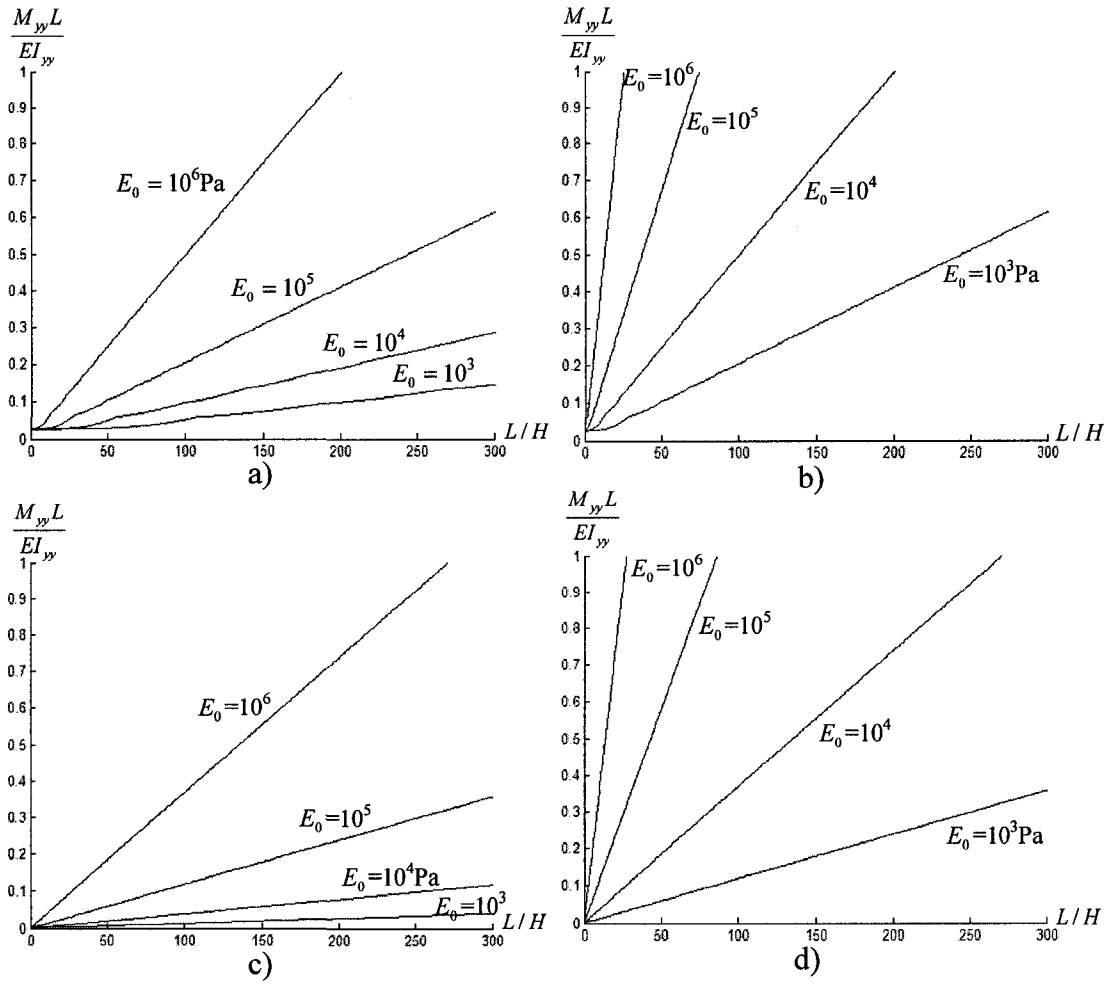

Fig. 3.1 The critical value for lateral buckling of the central pair under moment M_{yy} when a). G/E=10^{-3} and K_y=0.01 E_0, b). G/E=10^{-3} and $K_y = E_0$, c). G/E=10^{-5} and K_y=0.01 E_0, d). G/E=10^{-5} and $K_y = E_0$, where $\frac{M_{yy}L}{EI_{yy}}$ represents the ratio of the flagellum length to the radius of curvature of the bent flagellum.

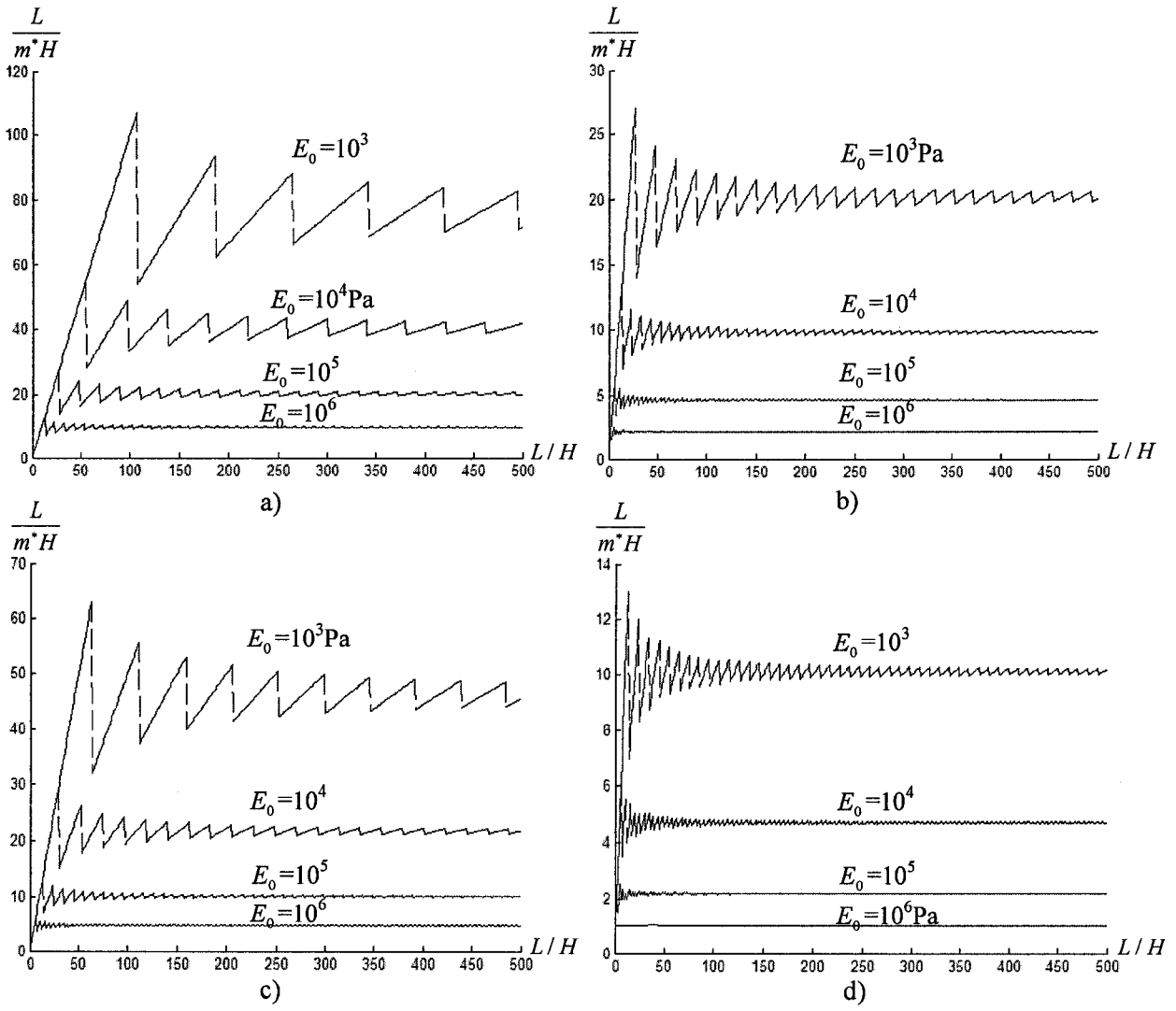

Fig. 3.2 The ratio of the buckling half-wavelength to the height H of the central pair for a). G/E =10^{-3} and K_y =0.01 E_0 , b). G/E =10^{-3} and K_y = E_0 , c). G/E =10^{-5} and K_y =0.01 E_0 , d). G/E =10^{-5} and K_y = E_0 .

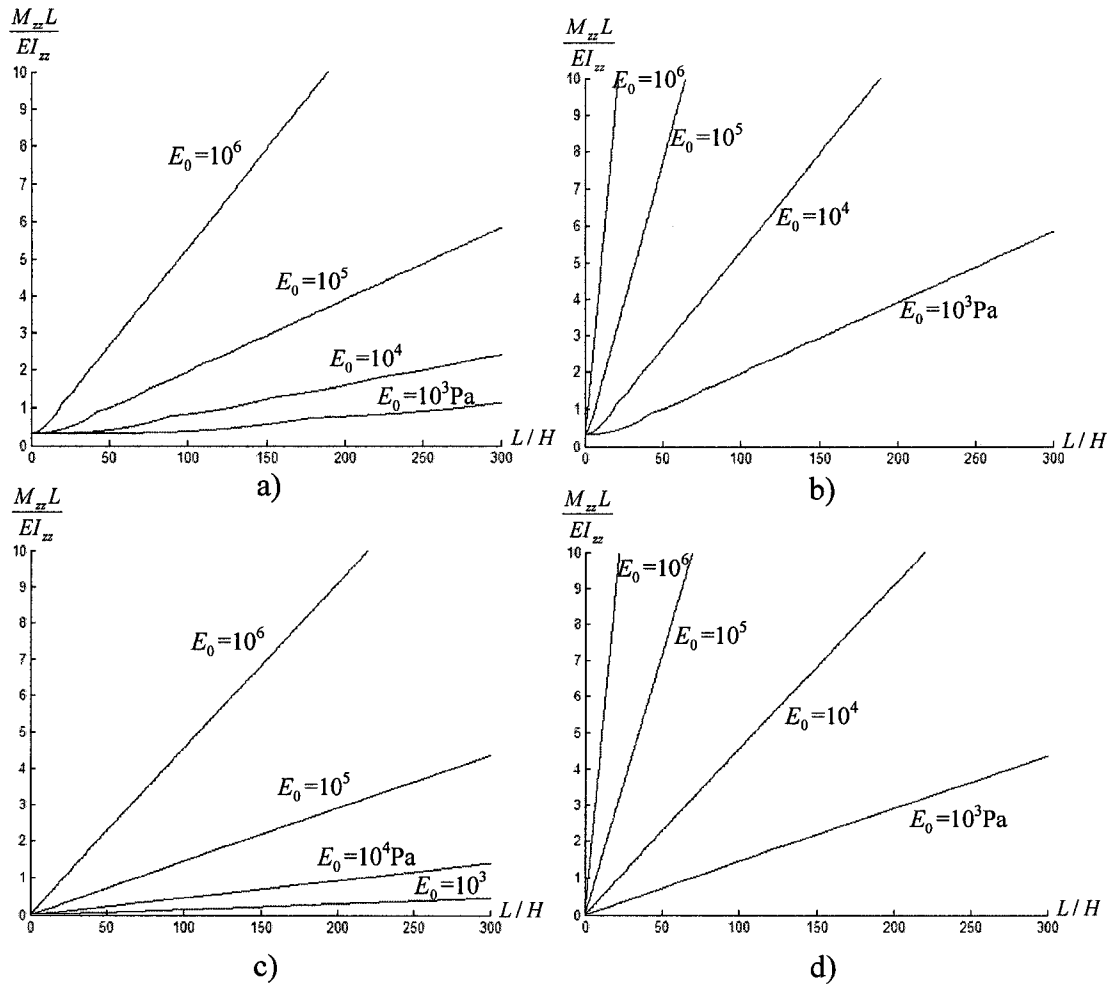

Fig. 3.3 The critical value for lateral buckling of the central pair under moment M_{zz} when a). $G/E=10^{-3}$ and $K_z=0.005\,E_0$, b). $G/E=10^{-3}$ and $K_z=0.5\,E_0$, c). $G/E=10^{-5}$ and $K_z=0.005\,E_0$, d). $G/E=10^{-5}$ and $K_z=0.5\,E_0$, where $\frac{M_{zz}L}{EI_{zz}}$ represents the ratio of the flagellum length to the radius of curvature of the bent flagellum.

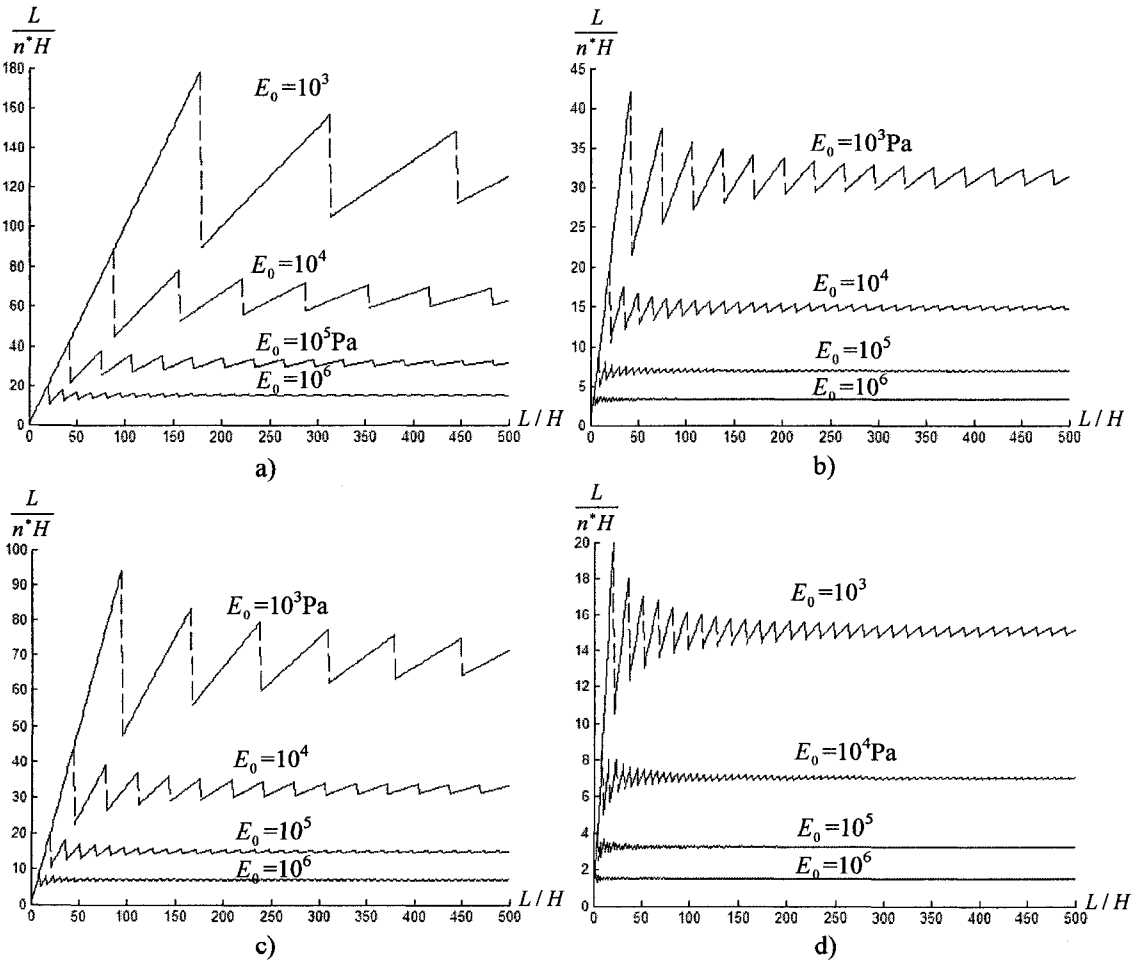

Fig. 3.4 The ratio of the buckling half-wavelength to the height H of the central pair for a). $G/E=10^{-3}$ and $K_z=0.005\,E_0$, b). $G/E=10^{-3}$ and $K_z=0.5\,E_0$, c). $G/E=10^{-5}$ and $K_z=0.005\,E_0$, d). $G/E=10^{-5}$ and $K_z=0.5\,E_0$.

Table 3.1 Critical radius of curvature and buckling wavelength when the central pair bent in the plane of maximum bending rigidity

Value of G, K_y, E_0	Critical radius of curvature	Buckling wavelength
$G/E=10^{-3}$, $K_y=0.01E_0$, $E_0=10^5 Pa$	30 μm	
$G/E=10^{-5}$, $K_y=0.01E_0$, $E_0=10^5 Pa$	50 μm	
$G/E=10^{-3}$, $K_y=E_0$, $E_0=10^4 Pa$	12 μm	
$G/E=10^{-5}$, $K_y=E_0$, $E_0=10^4 Pa$	15 μm	
$G/E=10^{-3}$, $K_y=E_0$, $E_0=10^3 Pa$		2.4 μm
$G/E=10^{-5}$, $K_y=E_0$, $E_0=10^3 Pa$		1.2 μm
$G/E=10^{-3}$, $K_y=0.01E_0$, $E_0=10^4 Pa$		4.8 μm
$G/E=10^{-5}$, $K_y=0.01E_0$, $E_0=10^4 Pa$		2.4 μm

Table 3.2 Critical radius of curvature and buckling wavelength when the central pair bent in the plane of minimum bending rigidity

Value of G, K_y, E_0	Critical radius of curvature	Buckling wavelength
$G/E=10^{-3}$, $K_y=0.01E_0$, $E_0=10^5 Pa$	3 μm	
$G/E=10^{-5}$, $K_y=0.01E_0$, $E_0=10^5 Pa$	4 μm	
$G/E=10^{-3}$, $K_y=E_0$, $E_0=10^3 Pa$	3 μm	4 μm
$G/E=10^{-5}$, $K_y=E_0$, $E_0=10^3 Pa$	4 μm	1.8 μm
$G/E=10^{-3}$, $K_y=0.01E_0$, $E_0=10^4 Pa$		9 μm
$G/E=10^{-5}$, $K_y=0.01E_0$, $E_0=10^4 Pa$		4 μm

Chapter 4

Length-dependence of the Flexural Rigidity of MTs

4.1 Introduction

As an elastic rod or beam, the flexural rigidity of a MT is expressed by ($E_x I$), where E_x is the longitudinal Young's modulus and I is the moment of inertia of the cross-section. The flexural rigidity of microtubule is the quality that describes an individual MT's resistance to elongation. For a spring, Hook's law states that force equals the product of stiffness by elongation. For a thin elastic rod, the analogous beam equation states that at each point bending moment equals the product of the flexural rigidity by the curvature. The flexural rigidity of an individual microtubule is completely determined by the properties of the bonds between the atoms within each protein subunit and properties of the bonds which hold the subunit together in the polymer [55]. As reviewed, the flexural rigidity of MTs and the Young's modulus were estimated using continuum (isotropic) elastic beam models from previous researchers, where measurement results have an unrelated spreading over a wide range.

Among the many measurements of flexural rigidity of MTs, some researchers found in their measurement of flexural rigidity, that flexural rigidity of MTs is not a constant parameter defining the flexural rigidity of a microtubule. They suggested that a length dependency of flexural rigidity of MTs exists; on the other hand, some researchers cannot confirm such length dependency by their measurement results of flexural rigidity. Regarding this problem, researchers made much effort to make it clear but until now they still have not known the exact reason behind this problem.

Indeed, among various factors affecting the measured flexural rigidity, the length of MTs has been identified by some as a key parameter [28, 29]. The reported lowest flexural rigidity and Young's modulus are always associated with very short MTs (of a few microns) [29, 56], while the reported higher flexural rigidity and Young's modulus are always associated with longer MTs (of a few tens of microns) [29, 55]. Therefore,

unlike the usual concept of length-independent flexural rigidity of elastic rods, it seems that MTs have a length-dependent flexural rigidity based on some of the previous various researches. This issue has caused considerable confusion and not been well addressed in the literature.

In the following, we will use the orthotropic shell model to quantitatively show that, when modeled as an elastic beam, the flexural rigidity of MTs does depend on their length, as a result of the strongly anisotropic elastic properties of MTs. The frequencies and critical buckling loads are predicted by the accurate orthotropic shell model and compared with those given by the approximate isotropic beam model. Also, a critical length of MTs beyond which the relative error of squared lowest frequency predicted by the isotropic beam model and the orthotropic shell model is less than 10% and 1% respectively is determined. Simultaneously, a critical length of MTs beyond which relative error of the lowest buckling load predicted by the isotropic beam model and the orthotropic shell model is less than 10% and 1% respectively is determined.

It is shown that vibration frequencies and buckling load predicted by the accurate orthotropic shell model are much lower than that given by the approximate isotropic beam model for shorter MTs, although the two models give almost identical results for sufficiently long MTs. It is this inaccuracy of the isotropic beam model used by all previous researchers that leads to reported lower flexural rigidity and Young's modulus for shorter MTs. In particular, much lower shear modulus and circumferential Young's modulus, which only weaken flexural rigidity of shorter MTs, are responsible for the observed length-dependence of the flexural rigidity. These results confirm that longitudinal Young's modulus of MTs is length-independent, and the observed length-dependence of the flexural rigidity and Young's modulus is a result of strongly anisotropic elastic properties of MTs which have a length-dependent weakening effect on flexural rigidity of shorter MTs.

4.2 Free vibration of MTs

In this section, free vibration of MTs will be discussed by using the orthotropic shell model. Particularly, we focus on beam-like free vibration of MTs in order to compare with that from the isotropic beam model.

4.2.1 Beam-like free vibration of MTs

To study free vibration of MTs, let us consider MTs with simply supported ends and then,

$$\begin{aligned} u(x,\theta,t) &= U\cos k_x x\cdot\cos n\theta\cdot e^{i\omega t} \\ v(x,\theta,t) &= V\sin k_x x\cdot\sin n\theta\cdot e^{i\omega t} \\ w(x,\theta,t) &= W\sin k_x x\cdot\cos n\theta\cdot e^{i\omega t} \end{aligned} \tag{4.1}$$

where U, V and W are some constants representing the vibration amplitudes in longitudinal, circumferential and radial directions, respectively, k_x ($k_x = \frac{m\pi}{L}$, m is a positive integer representing half axial wave number and L is the length of a MT) is the wave vector along longitudinal direction, n is the circumferential wave number, and ω is angular frequency which is related to frequency f by $\omega = 2\pi f$.

C.Y. Wang et al. [88] studied beamlike vibration of multi-walled carbon nanotubes based on a multi-shell model. They found that the multi-shell model is in good agreement with the multi-beam model for almost coaxial bending modes of large- or small-radius MWNTs and non-coaxial B modes of small-radius MWNTs (Multiwall Carbon Nanotubes). Also, when the wave vector decreases, the lowest frequency decreases and the associated mode shifts from R mode with larger n to a coaxial B mode with n=1. Inspired by this study, the beamlike vibration of MTs will be analyzed. Beamlike bending of a shell is defined by n =1 and $w = v$, where w and v represent radial and circumferential displacements of the shell, respectively. Here, we mention that, the calculation of the amplitude ratios is essential for classifying all frequencies into L, R, T or B modes because we can always get three frequencies for every m, n combination based on solving the governing equation. When MTs length is sufficiently long, the R mode corresponding to the lowest frequency will shift to B mode. So in the following analysis, we consider the wave vector ranging from 0.001 to 0.01 because MTs usually have length ranging from a few microns to a few tens of microns. Based on the beamlike vibration mode, we will compare the more accurate orthotropic shell model

with the isotropic beam model to further study the beamlike modes of microtubule vibration.

Let us first consider free vibration of a MT simply supported at its two ends. In order to examine the accuracy of the isotropic beam model, taking the circumferential number n=1 in equation (4.1), we consider beam-like vibration modes of shell model given by

$$\begin{aligned} u(x,\theta,t) &= U\cos k_x x\cdot\cos\theta\cdot e^{i\omega t} \\ v(x,\theta,t) &= V\sin k_x x\cdot\sin\theta\cdot e^{i\omega t} \\ w(x,\theta,t) &= W\sin k_x x\cdot\cos\theta\cdot e^{i\omega t} \end{aligned} \tag{4.2}$$

Substituting Eq. (4.2) into (2.15) leads to the following equation

$$H(\Omega,k)_{3\times 3}\cdot\begin{bmatrix} U \\ V \\ W \end{bmatrix} = 0 \tag{4.3}$$

where Ω ($=\dfrac{r\omega}{S_L}$) is dimensionless frequency and k ($=r\cdot k_x$) is dimensionless wave-vector. The existence condition of a nonzero solution of U, V and W determines the frequency Ω, as a function of the wave vector k.

4.2.2 Comparison with that predicted by isotropic beam model

For MTs we take r=12.8 nm, α =0.001, E_x =1 GPa , ν_x =0.3, and $\beta = \dfrac{G_{x\theta}}{E_x}$ varying between 0.000004 and 0.001 (see Table 2.2). Because MTs usually have lengths ranging from a few microns to a few tens of microns, we consider $\dfrac{m\pi r}{L}$ ranging from 0.001 to 0.01. First, it is seen from Fig. 4.1 that the isotropic beam model, used in all previous papers [28-29, 51-58], gives sufficiently accurate frequencies provided

β =0.001 and $\frac{m\pi r}{L}$ is less than 0.01. This concludes that, if β =0.001, frequencies predicted by the isotropic beam model are accurate enough for sufficiently long MTs (say, $\frac{m\pi r}{L}$ <0.01, or L>4m μm). Since square of frequency is proportional to the flexural rigidity or the (longitudinal) Young's modulus, it follows that, when β =0.001, the estimated flexural rigidity and (longitudinal) Young's modulus of MTs based on the lowest-frequency mode (m=1) are accurate enough for MTs of length longer than 4 μm . When higher-order modes are concerned, say m=3, the estimated flexural rigidity and (longitudinal) Young's modulus of MTs based on the first three modes are accurate enough for MTs of length longer than 12 μm .

However, as stated above, actual shear modulus of MTs is much lower than 1 MPa and then β should be much smaller than 0.001. For example, for β =0.0001 and β =0.00001, it is seen from Fig. 4.1 that the accurate frequencies of MTs, given by the present orthotropic shell model, are much lower than those predicted by the isotropic beam model for shorter MTs (say, $\frac{m\pi r}{L}$ >0.005, or L< 8m μm). In this case, when the isotropic beam model is used, the measured frequencies will lead to a much lower flexural rigidity or (longitudinal) Young's modulus. This can explain why some previously estimated values of the flexural rigidity and (longitudinal) Young's modulus, based on vibration analysis of MTs, are very low when the length of MTs is not sufficiently long.

4.2.3 Critical length of MTs based on free vibration

Here, it is interesting to determine a critical length of MTs beyond which the relative error of squared lowest frequency (m=1) predicted by the isotropic beam model and the orthotropic shell model (2.15) is less than 10%. Such a critical length is shown in Fig. 4.2 (solid line), as a function of the value of β . It is seen from Fig. 4.2 that the critical length is 12 μm if β =0.0001, or 38 μm if β =0.00001. This means that for MTs of length less than such a critical length, because the flexural rigidity is proportional to squared frequency, the estimated flexural rigidity will be more than 10% lower and thus the

estimated Young's modulus will be more than 10% lower than the actual longitudinal modulus E_x.

On the other hand, if a critical length of MTs is defined so that beyond which the relative error of squared lowest frequency predicted by the two models is less than 1%, the dependence of the critical length on β is shown in Fig. 4.3 (solid line). It is seen from Fig. 4.3 that the critical length becomes 36 μm if β =0.0001, or 40 μm if β=0.00008.

4.3 Static buckling of MTs

In this section, static buckling of MTs will be discussed by using the orthotropic shell model. Particularly, we focus on beamlike buckling modes in order to make a comparison with the isotropic beam model.

4.3.1 Axially compressed buckling of MTs

Let us now consider an axially compressed MT simply-supported at its two ends, such that:

$$u(x,\theta) = U\cos\frac{m\pi}{L}x\cdot\cos n\theta$$

$$v(x,\theta) = V\sin\frac{m\pi}{L}x\cdot\sin n\theta$$

$$w(x,\theta) = W\sin\frac{m\pi}{L}x\cdot\cos n\theta \qquad (4.4)$$

where U, V and W are some real constants, m is a positive integer representing half axial wave number, n is the circumferential number, and L is the length of microtubule.

Similar to Section 4.2.1, we will investigate the beamlike buckling modes of an individual microtubule in order to compare with the results obtained from previous isotropic beam model. An axial compression is applied on the microtubule. The critical buckling force required for axially compressed buckling with different wave vector can

be obtained. Similarly, in order to explore beamlike buckling modes of MTs and examine the accuracy of the isotropic beam model, we have to take sufficiently long MTs to analyze. So in the following we consider wave vector ranging from 0.001 to 0.01 that makes MTs long enough. Take the circumferential number n=1 in equation (4.4), the beamlike buckling modes are given by

$$u(x,\theta) = U\cos\frac{m\pi}{L}x\cdot\cos\theta$$

$$v(x,\theta) = V\sin\frac{m\pi}{L}x\cdot\sin\theta$$

$$w(x,\theta) = W\sin\frac{m\pi}{L}x\cdot\cos\theta \tag{4.5}$$

Substituting (4.5) into (2.16) yields the following equation

$$M\left(N_x,\frac{L}{m\pi r}\right)_{3\times3}\cdot\begin{bmatrix}U\\V\\W\end{bmatrix}=0 \tag{4.6}$$

The existence condition of a nonzero solution of (U,V,W) is $\det M = 0$ which determines buckling load.

4.3.2 Comparison with that predicted by isotropic beam model

Similar to vibration, we take r=12.8nm, α =0.001, E_x=1 GPa, ν_x=0.3, and β varying between 0.000004 and 0.001. The critical buckling load N_{cr} for axially compressed buckling is plotted in Fig. 4.4 for $\frac{m\pi r}{L}$ ranging from 0.001 to 0.01, with a comparison to the results given by the isotropic elastic beam model (dashed line). First, it is seen from Fig.4.4 that the isotropic beam model gives sufficiently accurate frequencies if β=0.001 and $\frac{m\pi r}{L}$ is less than 0.01. This concludes that, if β=0.001, the lowest buckling load (m=1) predicted by the isotropic beam model is accurate enough for longer

MTs (say, $\frac{\pi r}{L}$ <0.01, or L>4 μm). Since the buckling load is proportional to the flexural rigidity or (longitudinal) Young's modulus, it follows that, when β =0.001, the estimated flexural rigidity and Young's modulus of MTs are accurate enough for MTs of length $\geq 4\,\mu m$.

However, for the more realistic values of β, such as β=0.0001 and 0.00001, it is seen from Fig.4.4 that the actual (lowest) buckling load of MTs (m=1), given by the present shell model, is much lower than that predicted by the isotropic beam model for shorter MTs (say, $\frac{\pi r}{L}$ >0.005, or L<8 μm). In this case, the measured lower buckling load will lead to a lower flexural rigidity or (longitudinal) Young's modulus if the isotropic beam model is used. This explains why previously estimated flexural rigidity and Young's modulus of MTs, based on buckling load of MTs, are very low when the length of MTs is not sufficiently long.

4.3.3 Critical length of MTs based on buckling

Similar to vibration, a critical length of MTs beyond which relative error of the lowest buckling load predicted by the isotropic beam model and the orthotropic shell model (2.16) is less than 10%, is shown in Fig.4.2 (dash line). It is seen from Fig.4.2 that the critical length determined by the buckling load (dash line) is coincident with the critical length determined by the vibration frequencies (solid line). For example, just like the critical length determined by vibration analysis, the critical length is also 12 μm if β =0.0001, or 38 μm if β =0.00001. Furthermore, if the critical length of MTs is defined so that beyond which relative error of the buckling load predicted by the two models is less than 1%, the dependence of the critical length on β is shown in Fig. 4.3 (dash line). Again, the solid line and the dash line are coincident. Thus, the critical length for relative error less than 1% is also 36 μm if β =0.0001, or 40 μm if β =0.00008.

4.4 Comparison with existing experimental data and a known formula

In this section, we will give existing results on length-independent flexural rigidity and make a comparison of results from the present shell model with existing experimental data and a known formula.

4.4.1 Existing results on length-independent flexural rigidity

MTs play an important role in determining cell shape and polarity and are required to have suitable flexural rigidity. That is why many researchers make every effort to estimate the flexural rigidity of MTs. Among various methods, there are two experiments which have given us important experimental data on flexural rigidity of MTs. Kurachi et al. [28] measured the flexural rigidity of a single microtubule by direct buckling using the optical trapping technique. There are three ways of estimating the flexural rigidity of a continuous slender rod, one is from the observed critical load of buckling and the other two are from deflected lengths and angles of bending, resulting in values which agreed well when applied to analysis of buckling MTs. Some representative data is taken from Kurachi et al. (see fig. 5 of [28]) and is shown in Table 4.1.

Pampaloni et al. in [64] stated that, on the mesoscopic length scale of a cell, their material properties are characterized by a single parameter, the persistence length. So they use single-particle tracking methods combined with a fluctuation analysis to systematically study the dependence of persistence on the microtubule lengths. Some representative data is taken from Pampaloni et al. (see fig. 3 of [64]) and shown in Table 4.2.

In addition to the above existing experimental data, there is a formula derived from [53, 61] (see eqn. (2) of [53] or [61]) as follows

$$\frac{E_B}{E} = \frac{1}{1 + \dfrac{10(D_{ext} + D_{\text{int}})^2}{3\beta L^2}} \tag{4.7}$$

where E_B is the length-dependent bending modulus, E is Young's modulus, D_{ext} and D_{int} are respectively the microtubule's external and internal diameters, L is the length of

a single microtubule, $\beta = G/E$ and G is the shear modulus. The length-dependence of flexural rigidity can also be predicted by this formula.

In contrast, Flegner et al. reported no length dependence of flexural rigidity by measuring the dynamics of the microtubule in liquid. The length dependent flexural rigidity indicates that the conventional simple strength of material theory does not hold in measuring the flexural rigidity of MTs. The length dependence is a result of anisotropic elastic properties of MTs.

4.4.2 Comparison with experimental data and a known formula

Since squared frequency of an isolated MT (with N_x=0) is proportional to the flexural rigidity (EI) (through the relation $\omega^2 = \frac{EI}{\rho A}\cdot(\frac{m\pi}{L})^4$ [89]), the results of squared frequency can be used to study the length-dependence of flexural rigidity of MTs. The length-dependent flexural rigidity predicted by the orthotropic shell model, which is obtained by the squared frequency given by the orthotropic model divided by the squared frequency given by the classic beam model, is shown in Fig. 4.5. It is seen from Fig.4.5 that when β =0.0001 or smaller, flexural rigidity predicted by the orthotropic shell model changes more than one order of magnitude when the length of MTs changes from a few microns to a few tens of microns. In particular, when β =0.000001, flexural rigidity predicted by the orthotropic shell model changes almost three orders of magnitude when the length of MTs changes from a few microns to a few tens of microns. Therefore, the orthotropic shell model could explain the length-dependent flexural rigidity of MTs reported in the literature [28, 29, 53, 61, 64, 66] provided an appropriate value of β is used.

To compare the flexural rigidity predicted by the orthotropic shell model with that from experimental data, We also calculated the ratio of flexural rigidity from [28], which is obtained by flexural rigidity given by experiments divided by the limit value of flexural rigidity for infinitely long MTs, and the ratio of persistence length from [64], which is obtained by persistence length given by experiments divided by the limit value of

persistence length for infinitely long MTs. The ratios are shown in the Table 4.1 and Table 4.2, and plotted in the Fig. 4.5 as well.

Qualitatively, as shown in Fig. 4.5, the length-dependence of flexural rigidity predicted by the orthotropic shell model is consistent with experimental results reported in [28, 64] (see fig.5 of [28] and fig.3 of [64]). This proves that anisotropy of MTs and orthotropic shell model is more accurate for predicting the buckling loads and vibration frequencies of MTs than the beam model applied before in the previous research.

Here, in Fig. 4.5, the length-dependence of flexural rigidity predicted by the orthotropic shell model is also compared to that given by a formula (4.7). It is seen from Fig. 4.5 that the length-dependence of flexural rigidity predicted by the orthotropic shell model is consistently different from that given by the formula of [53, 61] by about one order of magnitude when the same value of β is used. Since the formula (4.7) suggested in [53] was based on a simplified analysis, it does not offer a unified theoretical model for static and dynamic mechanics of MTs, therefore, the orthotropic shell model developed here can be used as an adequate unified theoretical shell model. In particular, it is seen from Fig. 4.5 that the length-dependence of flexural rigidity predicted by the orthotropic shell model is in good quantitative agreement with experimental data reported in [28, 64] when the effective shear modulus of MTs is five to six orders of magnitude lower than the longitudinal modulus and thus the value of β is between 0.000001 and 0.00001 as suggested by some previous works [63, 64, 66].

4.5 Summary and discussion

In summary, the above results indicate that the length-dependence of the flexural rigidity of MTs for free vibration and buckling analysis can be well explained by the length-dependence of the accuracy of the isotropic beam model. Strongly anisotropic elastic properties of MTs are responsible for the observed length-dependence of the flexural rigidity of shorter MTs.

An accurate orthotropic elastic shell model for MTs was employed to study unexplained length-dependence of flexural rigidity and Young's modulus of MTs reported in the literature. It is shown that when the length of MTs reduces from a few tens of microns to a few microns, vibration frequencies and buckling load predicted by the

accurate orthotropic shell model are much lower than that given by the approximate isotropic beam model used by all previous related works. This inaccuracy of the isotropic beam model is responsible for reported lower values of flexural rigidity or longitudinal Young's modulus of shorter MTs. In particular, the present results confirm that the longitudinal Young's modulus of MTs is length-independent. The reported length-dependence of flexural rigidity or longitudinal Young's modulus of MTs is attributed to much lower shear modulus and circumferential Young's modulus which have a significant weakening effect on shorter MTs, while this weakening effect vanishes for sufficiently long MTs.

Indeed, the length-independent flexural rigidity of an isolated MT predicted by the orthotropic shell model is in good quantitative agreement with known experimental data when the effective shear modulus of MTs is five to six orders of magnitude lower than the longitudinal modulus as suggested by some previous works.

Here, it should be stated that flexural rigidity of MTs would depend not only on their lengths, but also on other conditions (such as added taxol[59] or growth/shrink velocity of MTs [90]). However, the present analysis clearly shows that the length of MTs will be definitely one of the dominant factors controlling the flexural rigidity of MTs.

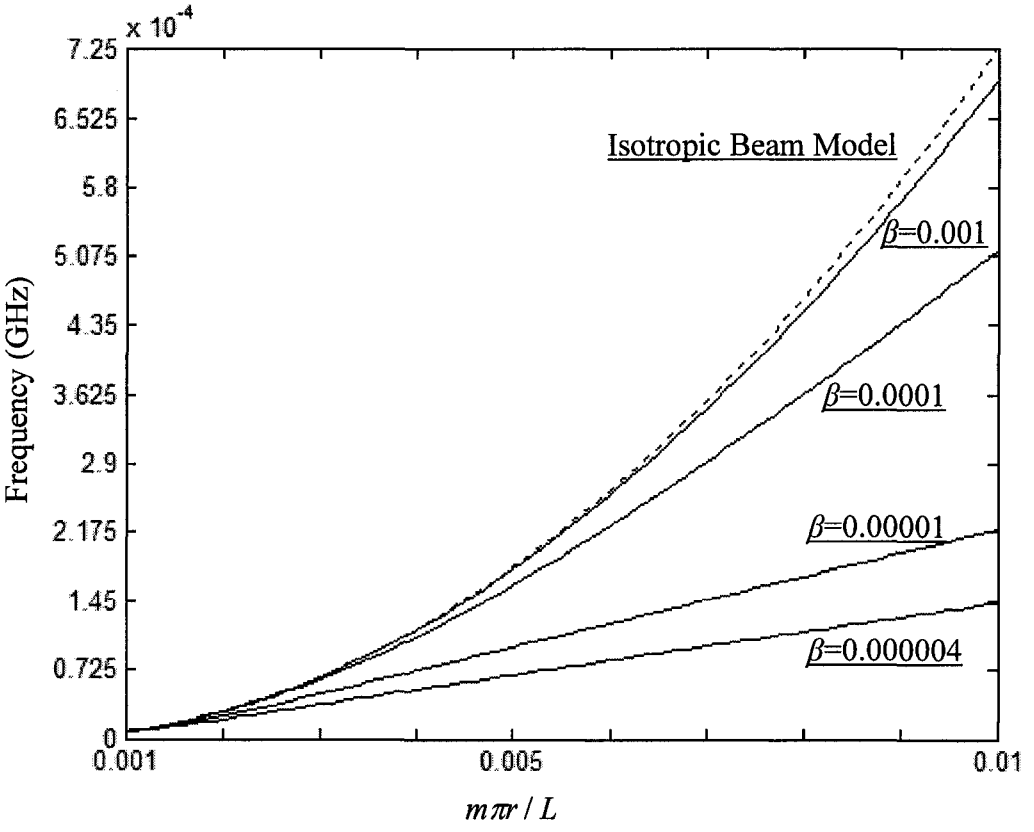

Fig. 4.1 Dispersion relation of MTs given by the orthotropic shell model (2.15) with comparison to that predicted by the isotropic beam model (dash line).

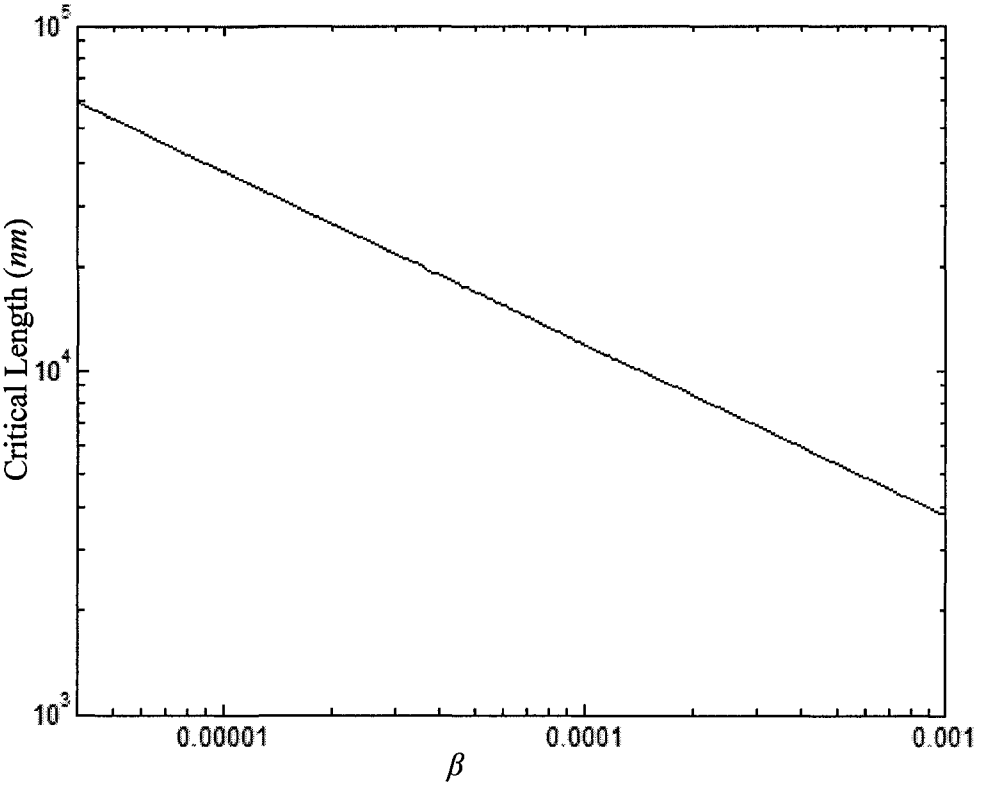

Fig. 4.2 A critical length of MTs beyond which the relative error of squared lowest frequency (m =1) predicted by the isotropic beam model and the accurate orthotropic shell model is less than 10%.

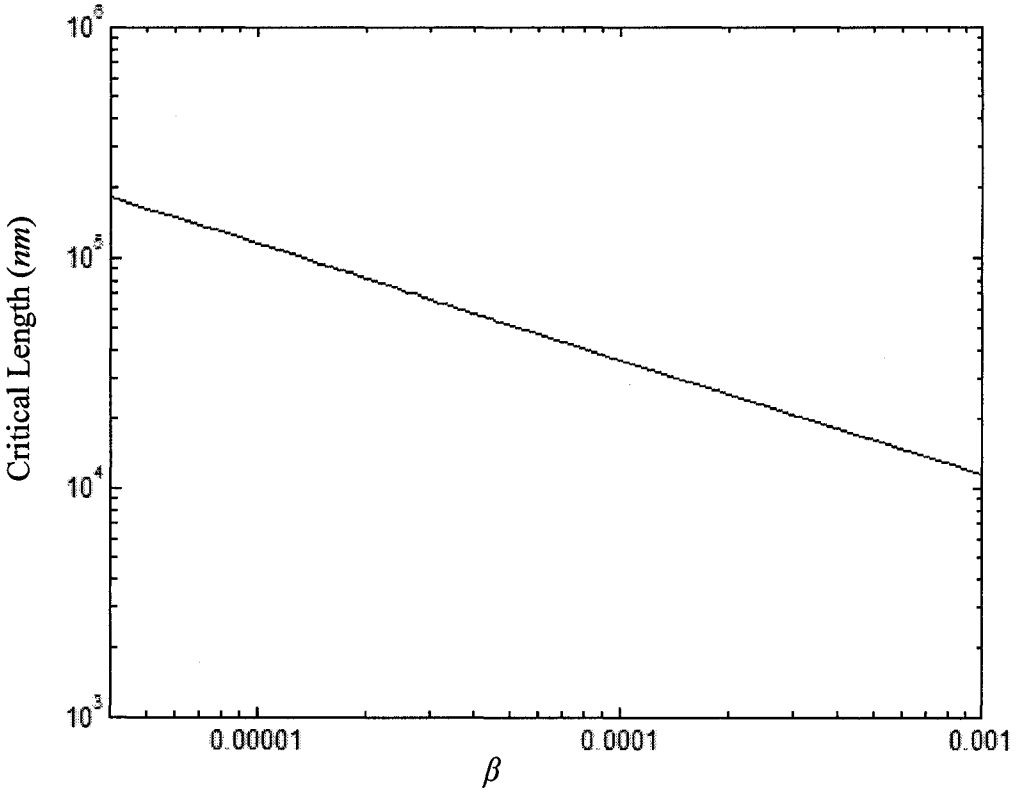

Fig. 4.3 A critical length of MTs beyond which the relative error of squared lowest frequency (m =1) predicted by the isotropic beam model and the accurate orthotropic shell model is less than 1%.

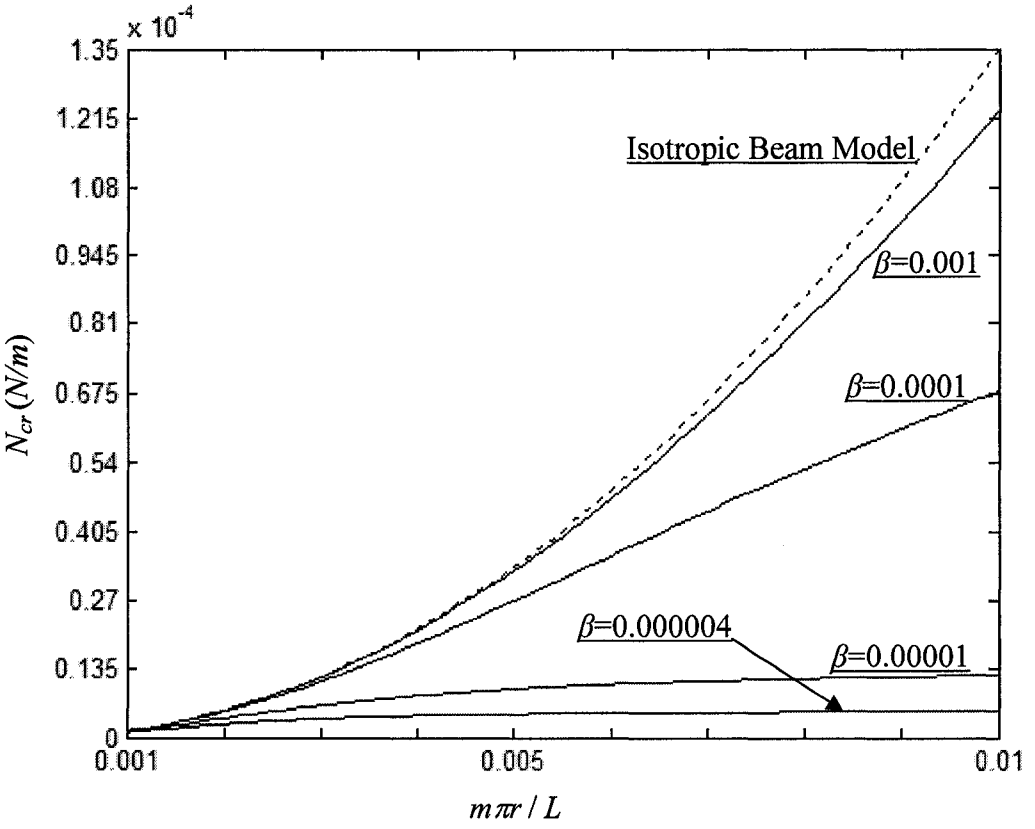

Fig. 4.4 Buckling load for axially compressed MTs given by the orthotropic shell model (2.16) with comparison to that predicted by the isotropic beam model (dash line).

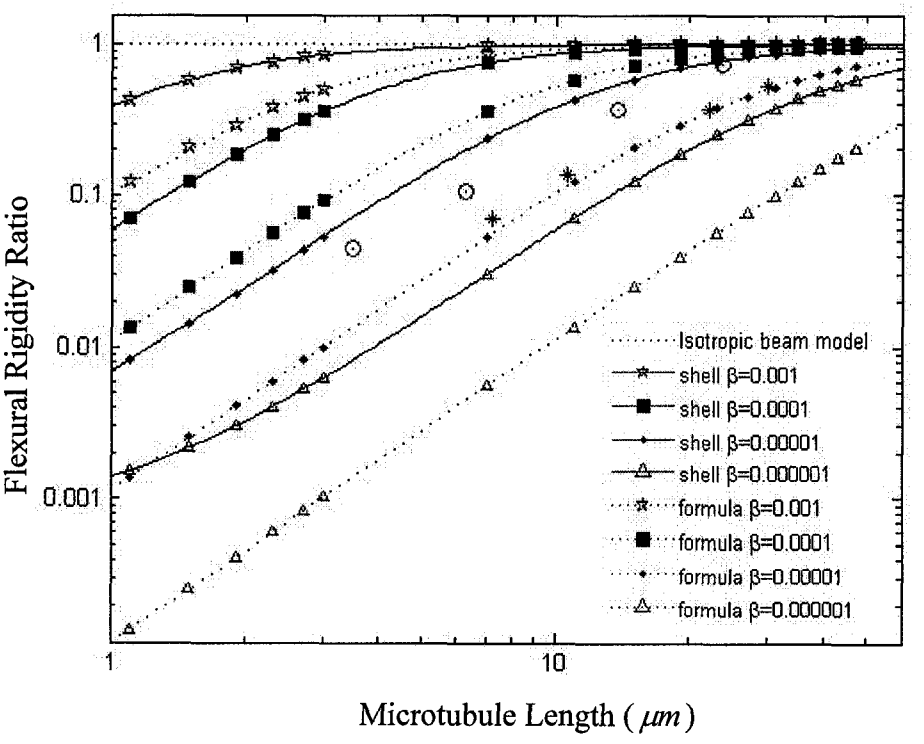

Fig. 4.5 Comparison between the flexural rigidity-length relations of an isolated MT given by the orthotropic shell model, the isotropic beam model, formula (4.7) used in [53] and experimental data ($*$ Experimental data from fig.5 of [28] and $\odot$ Experimental data from fig.3 of [64]) (Here the flexural rigidity is non-dimensionalized by the limit value of flexural rigidity for infinitely long MTs).

Table 4.1 The ratio of flexural rigidity of MTs obtained by experiments and the limit value of flexural rigidity for infinitely long MTs

Length of MTs (μm)	7.2	10.6	22.16	30
Flexural rigidity of MTs obtained by experiments ($N \cdot m^2$)	2.1×10^{-23}	4.05×10^{-23}	1.2×10^{-22}	1.6×10^{-22}
The limit value of flexural rigidity for infinitely long MTs ($N \cdot m^2$)	3×10^{-22}			
The ratio	0.07	0.135	0.4	0.5333

Table 4.2 The ratio of persistence length of MTs obtained by experiments and the limit value of persistence length for infinitely long MTs

Length of MTs (μm)	3.5	6.24	13.8	23.6	47.5
Persistence length of MTs obtained by experiments (μm)	225	538	1868	3703	5000
The limit value of persistence length for infinitely long MTs (μm)	5035				
The ratio	0.0447	0.1068	0.371	0.7355	0.9930

Chapter 5

Conclusions and Future Plans

In this thesis, a thin-walled elastic beam model was used to study why the central pair of eukaryotic flagella twists under bending, which is still unclear in previous literatures. As a whole, the central pair of MTs, including the bridge linking the two MTs, is described as a single elastic beam of thin-walled cross-section, assuming that the two MTs of the central pair are initially parallel to each other. The effects of all surrounding links and organelles inside the flagellum are modeled approximately by an equivalent surrounding elastic medium, defined by two spring constants for transverse deflections of the central pair and one spring constant for torsion of the cross-section of the central pair. Thus this novel elastic beam model gives us a new insight into the relationship between the central pair twisting and the flagella bending.

Meanwhile, an accurate orthotropic elastic shell model for MTs was employed to study unexplained length-dependence of flexural rigidity and Young's modulus of MTs reported in the literature while the elastic beam model was used most part in measuring the flexural rigidity of MTs. Vibration frequencies and buckling load of MTs were predicted by this accurate orthotropic shell model. In particular, it was found that vibration frequencies and buckling loads predicted by this orthotropic shell model are in good agreement with available experimental data. The major conclusions based on these two models are summarized and future plans are discussed in the following sections.

5.1 Conclusions

(1) Regarding the torsion of the central pair MTs in eukaryotic flagella due to bending-driven lateral buckling, we can conclude that:

a. A thin-walled elastic beam model was suggested to study bending-driven torsional/lateral buckling of the central pair MTs in eukaryotic flagella.

b. Torsion of the central pair will inevitably occur, as a result of bending-driven lateral buckling of the central pair.

c. Critical values and the wave-lengths predicted by the present model are comparable to available data.

d. The bending-driven torsion of the central pair studied in the present paper reveals an important aspect of torsion of the central pair which has not been realized in all previous works.

(2) Regarding length-dependence of the flexural rigidity as a result of anisotropic elastic properties of MTs, we can conclude that:

a. The vibration frequencies and buckling load predicted by the accurate orthotropic shell model are much lower than those given by the approximate isotropic beam model for shorter MTs, although the two models give almost identical results for sufficiently long MTs.

b. When the length of MTs reduces from a few tens of microns to a few microns, vibration frequencies and buckling loads predicted by the accurate orthotropic shell model are lower than that given by the approximate isotropic beam model by more than one order of magnitude.

c. The reported length-dependence of flexural rigidity or longitudinal Young's modulus of MTs is attributed to the much lower shear modulus and circumferential Young's modulus which have a significant weakening effect on shorter MTs, while this weakening effect vanishes for sufficiently long MTs.

d. The length-dependence of flexural rigidity predicted by the present orthotropic shell model is in good agreement with known experimental data.

5.2 Future plans

In this thesis, a novel beam model has been used for lateral/torsion buckling of the central pair, and an accurate orthotropic shell model was used for elastic buckling and free vibration of an individual microtubule. The beam model and the orthotropic shell model provide an alternative and effective method for studying mechanical behaviours and properties of the biological structure in the biomechanics field. Although much progress is made in experimental techniques, they are expensive and very difficult to run. Thus, it is anticipated that the beam model and the orthotropic shell model could be further utilized in the biomechanics field for the study of mechanical behaviour of structures like MTs. For example, in Chapter 3, we conducted our torsional buckling analysis on the basis of static pure bending, and so the thin-walled beam model is subjected to this limitation, but actual bending of flagella is always dynamic in nature and characterized by time-dependent and spacially non-uniform bending moment, on the other hand, the present analysis is restricted to linearized small deflections of the flagellum and small rotations of the central pair. So, in the next step, we will analyze the dynamic and geometrically nonlinear effects on bending-driven torsional buckling of the central pair. The above plans constitute a few interesting topics for further research.

The other plan is to analyze vibration frequencies and modes of a doublet of a certain length L. Regarding this plan, we have already had a specific idea. As reviewed in Section 1.1.2, microtubule doublet consists of a complete singlet microtubule, the A-tubule and an incomplete microtubule, the B-tubule. Unlike singlet MTs which are circular in cross-section, the A-tubules show a slight elliptical deformation with an elongation of about 8% in the axeneme's radial dimension. The configuration of the proteins appears to be designed to stabilize and maintain the protofilament architecture of the doublet as doublets undergo the stresses involved in axoneme motion and also to favor bending in the direction that corresponds to twisting of the axoneme. This will be a basis for quantitative modeling of mechanical properties. We are planning to model the doublets in our future work based on this structural configuration. The geometry of the doublets can be assumed to be a complete circle plus an ellipse, which is a relatively accurate description of doublets. We will analyze torsional/bending coupled vibration of

the doublets and find all frequencies and modes of the doublets' vibration. Based on vibration analysis we will explore what role the doublets play in flagella bending. In general, there are quite a few interesting topics about mechanics of MTs which still need to be investigated.

References

[1] N. E. Lamb, Cell Biology and Genetics, Mosby, Elsevier Inc. (2007)

[2] B. Lewin, L. Cassimeris, V.R. Lingappa, G. Plopper, Cells, Jones and Bartlett publishers, Sudbury, Massachusetts (2007)

[3] Y.M. Sirenko, M.A. Stroscio, and K.W. Kim, Elastic vibration of microtubules in a fluid, Phys. Rev. E 53 (1996) 1003.

[4] S. Portet, J.A. Tuszynski, C.W.V. Hogue and J.M. Dixon, Elastic vibrations in seamless microtubules, European Biophysics Journal 34 (2005) 912.

[5] J. Howard & A.A. Hyman, Dynamics and mechanics of the microtubule plus end, Nature 422 (2003)753.

[6] T. Watanabe, J. Noritake, K. Kaibuchi, Regulation of microtubules in cell migration, Trends in Cell Biology 15 (2005) 76.

[7] E. Nogales, Structural insights into microtubule function, Annual Review Biochemistry 69 (2000) 277.

[8] J. Howard, Mechanics of motor proteins and the cytoskeleton, Sinauer Associates, Inc. Sunderland (2001).

[9] R. Cotterill, Biophysics –an introduction, John Wiley, New York (2002).

[10] D. Boal, Mechanics of the cell, Cambridge Univ. Press., Cambridge (2002).

[11] I.R. Gibbons, Cilia and flagella of eukaryotes, J. Cell Biology 91(1981) 107.

[12] C.J. Brokaw, Bending-wave propagation by microtubules and flagella, Mathematical Biosciences 90 (1988) 247.

[13] M. Schliwa and G. Woehlke, Molecular motors, Nature 422 (2003) 759.

[14] N.J. Carter and R.A. Cross, Mechanics of the kinesin step, Nature 435 (2005) 308.

[15] J.M. Scholey, I. Brust-Mascher & A. Mogilner, Cell division, Nature 422(2003) 746.

[16] J. Lighthill, Flagellar hydrodynamcis, SIAM Review 18 (1976) 161.

[17] F.D. Warner, and P. Satir, The substructures of ciliary microtubules, J. Cell Sci. 12 (1973) 313.

[18] J.L. Rosenbaum & G.B. Witman, Intraflagellar transport, Nature Reviews, Molecular Cell Biology 3 (2002) 813.

[19] R. A. Bloodgood, Ciliary and Flagellar Membranes, Plenum Press, New York (1990).

[20] C.K. Omoto and C. Kung, The pair of central tubules rotates during ciliary beat in paramecium, Nature 279 (1979) 534.

[21] D.R. Mitchell and M. Nakatsugawa, Bend propagation drives central pair rotation in Chlamydomonas reinhardtii flagella, J. Cell Biology 166 (2004) 709.

[22] H.X. Sui & K.H. Downing, Molecular architecture of axonemal microtubule doublets revealed by cryo-electron tomography, Nature 442 (2006) 475

[23] P. Hannon, K. Knapp, Forensic Biomechanics, Lawyers & Judges Publishing Company, Inc. (2006)

[24] A. Richard, M.D. Brand, Davies F. P., Cell Biomechanics, J. Biomechanics 29 (1996) 389.

[25] C.T. Lim, E.H. Zhou, S.T. Quek, Mechanical models for living cells- a review, J. of Biom. 39 (2006) 195.

[26] J.E. Schoutens, Predictions of elastic properties of sperm flagella, J. Theore. Biology 171 (1994) 163.

[27] D.J. Odde, L. Ma, Microtubule bending and breaking in living fibroblast cells, Journal of Cell Science 112 (1999)3283.

[28] M. Kurachi, M. Hoshi and H. Tashiro, Buckling of a single microtubule by optical trapping forces: Direct measurement of microtubule rigidity, Cell Motility and the Cytoskeleton 30 (1995) 221.

[29] T. Takasone, S. Juodkazis, Y. Kawagishi, A. Yamaguchi, S. Matsuo, H. Sakakibara, H. Nakayama, and H. Misawa. Flexural rigidity of a single microtubule, Japaness J. Appl. Phys. 41 (2002) 3015.

[30] K.E. Machin, Wave propagation along flagella, J. Exp. Biology 35 (1958) 796.

[31] C.J. Brokaw, Bend propagation along flagella, Nature 209 (1966) 161.

[32] G.G. Vernon & D.M. Woolley, Microtubule displacements at the tips of living flagella, Cell Motility & Cytoskeleton 52 (2002) 151.

[33] C.B. Lindemann, Structural-functional relationships of the dynein, spokes, and central-pair projections predicted from an analysis of the forces acting within a flagellum, Biophy. J. 84 (2003) 4115.

[34] J.E. Schoutens, A model describing bending in flagella, J. Biological Phys. 30 (2004) 97.

[35] C. Cibert & J.V. Heck, Geometry drives the deviated-bending of the bi-tubular structure of the 9+2 axoneme in the flagellum, Cell Motility & Cytoskeleton 59 (2004) 153.

[36] J. Gray & G.J. Hancock, The propulsion of sea-urchin spermatozoa, J. Exp. Biology 32 (1955) 802.

[37] C. Brennen & H. Winer, Fluid mechanics of propulsion by cilia and flagella, Annual Review. Fluid. Mech. 9 (1977) 339.

[38] C.H. Wiggins, D. Riveline, A. Ott & R.E. Goldstein, Trapping and wiggling: elastohydrodynamics of driven microfilaments, Biophy. J. 74 (1998) 1043.

[39] R.H. Dillon & L.J. Fauci, An intergrative model of internal axoneme mechanics and external fluid dynamics in ciliary beating, J. Theore. Biology 207 (2000) 415.

[40] C.J. Brokaw, Simulating the effects of fluid viscosity on the behavior of sperm flagella, Math. Method. Applied Sci. 24 (2001) 1351.

[41] M. Kim and T.R. Powers, Hydrodynamic interaction between rotating helices, Phy. Rev. E 69 (2004) 061910.

[42] M. Manghi, X. Schlaberger & R.R. Netz, Propulsion with rotating elastic nanorods, Phy. Rev. Let. 96 (2006) 068101.

[43] C.K. Omoto and G.B. Witman, Functionally significant central-pair rotation in a primitive eukaryotic flagellum, Nature 290 (1981) 708.

[44] D.M. Woolley and G.G. Vernon, Alternative torsions in a living "9+2" flagellum, Pro. R. Soc. Lond B 266 (1999) 1271.

[45] C.K. Omoto, Rotation of the central pair microtubules in Eukaryotic flagella, Molecular Biology of the Cell 10 (1999) 1.

[46] C. Cibert, Axonemal activity relative to the 2D/3D-waveform conversion of the flagellum, Cell Motility & Cytoskeleton 51 (2002) 89.

[47] D.R. Mitchell, Orientation of the central pair complex during flagellar bend formation in Chlamydomonas, Cell Motility & Cytoskeleton 56 (2003) 120.

[48] M.J. Wargo and E.F. Smith, Asymmetry of the central apparatus defines the location of active microtubule sliding in flagella, Proc. Nat. Aca. Sci. 100 (2003) 137.

[49] K.A. Wemmer and W.F. Marshall, Flagellar motility: All pull together, Current Biology 14 (2004) R992.

[50] R. Yokoyama, E.O. Toole, S. Ghosh and D.R. Mitchell, Regulation of flagellar dynein activity by a central pair kinesin, Proc. Nat. Aca. Sci. 101 (2004) 17398.

[51] N. Wang, K. Naruse, D. Stamenovic, J.J. Fredberg, S.M. Mijailovich, I.M. Tolic-Norrelykke, T. Polte, R. Mannix and D.E. Ingber, Mechanical behavior in living cells consistent with the tensegrity model, Proceedings of the National Academy of Sciences 98 (2001) 7765.

[52] S. Kasas, C. Cibert, A. Kis, P.D.L. Rios, B.M. Riederer, L. Forro, G. Dietler and S. Catsicas, Oscillation modes of microtubules, Biology of the Cell 96 (2004) 697.

[53] S. Kasas, A. Kis, B.M. Riederer, L. Forro, G. Dietler and S. Catsicas, Mechanical properties of microtubules explored using the finite elements method, Chem. Phys. Chem 5 (2004) 252.

[54] P. Venier, A.C. Maggs, M.F. Carlier and D. Pantaloni, Analysis of microtubule rigidity using hydrodynamic flow and thermal fluctuations, Journal of Biological Chemistry 269 (1994) 13353.

[55] F. Gittes, B. Mickey, J. Nettleton and J. Howard, Flexural rigidity of microtubules and actin filaments measured from thermal fluctuation in shape, The Journal of Cell Biology 120 (1993) 923.

[56] A. Vinckier et al., Dynamical and mechanical study of immobilized microtubules with atomic force microscopy, J. Vac. Sci. Technolo. B14 (1996) 1427.

[57] J.A. Tolomeo & M.C. Holley, Mechanics of microtubule bundles in pillar cells from the inner ear, Biophy. J. 73 (1997) 2241.

[58] M. Kikumoto, M. Kurachi, V. Tosa and H. Tashiro, Flexural rigidity of individual microtubules measured by a buckling force with optical traps, Biophysical Journal 90 (2006) 1687.

[59] H. Felgner, R. Frank and M. Schiwa, Flexural rigidity of microtubules measured with the use of optical tweezers, Journal of Cell Science 109 (1996) 509.

[60] M. Elbaum, D.K. Fygenson, and A. Libchaber, Buckling microtubules in vesicles, Physical Review letters 76(21) (1996) 4078.

[61] A. Kis, S. Kasas, B. Babic, A.J. Kulik, W. Benoît, G.A.D. Briggs, C. Schönenberger, S. Catsicas, L. Forró, Nanomechanics of microtubules, Phys. Rev. Let. 89 (2002) 248101.

[62] P.J. Pablo, LAT Schaap, F.C. Mackintosh and C.F. Schmit, Deformation and collapse of microtubules on the nanometer scale, Phy. Rev. Let. 91 (2003) 098101.

[63] J.A. Tuszynski, T. Luchko, S. Portet and J.M. Dixon, Anisotropic elastic properties of microtubules, Eur. Phys. J. E17 (2005) 29.

[64] F. Pampaloni, G. Lattanzi, A. Jonas, T. Surrey, E. Frey, and E.-L. Florin, Thermal fluctuations of grafted microtubules provide evidence of a length-dependent persistence length, PNAS 103(2006)10248.

[65] C. Li, C.Q. Ru, and A. Mioduchowski, Torsion of the central pair microtubules in eukaryotic flagella due to bending-driven lateral buckling, Biochemical and Biophysical Research Communications 351(1) (2006) 159.

[66] C. Li, C.Q. Ru, A. Mioduchowski, Length-dependence of flexural rigidity as a result of anisotropic elastic properties of microtubules, Biochemical and Biophysical Research Communications 349(3) (2006) 1145.

[67] S.O. Timoshenko and J.M. Gere, Theory of elastic stability, McGraw-Hill, New York (1961).

[68] A. Chajes, Principles of structural stability theory, Prentice-Hall, Englewood Cliffs, NJ (1974).

[69] R.L. Serrette and T. Pekoz, Distorsional buckling of thin-walled beams/panels, J. Structural Engng. 121 (1995) 757.

[70] J.G. Teng, J. Yao and Y. Zhao, Distorsional buckling of channel beam-columns, Thin-walled Structures 41 (2003) 595.

[71] R.D. Cook and W.C. Young, Advanced mechanics of materials (2nd edition), Prentice Hall. New Jersey 1999.

[72] W.B. Bickford, Advanced mechanics of materials, Addison-Wesley. Menlo Park, California. 1998.

[73] G. Bao & S. Suresh, Nature Materials. 2 (2003) 715.

[74] J. Yoon, C.Q. Ru and A. Mioduchowski, Vibration of an embedded multiwall carbon nanotube, Composites Sci. Tech. 63 (2003) 1533.

[75] C.Q. Ru, Elastic models for carbon nanotubes, Encyclopedia of Nanoscience and Nanotechnology (ed. HS Nalwa), American Scientific Publishers, Vol.2 (2004) 731.

[76] E. Nogales, M. Whittaker, R.A. Milligan and K.H. Downing, High-resolution model of the microtubule, Cell 96 (1999) 79.

[77] V. VanBuren, D.J. Odde and L. Cassimeris, Estimates of lateral and longitudinal bond energies within the microtubule lattice, Proceedings of the National Academy of Sciences 99 (2002) 6035.

[78] D.J. Needleman, M.A. Ojeda-Lopez, U. Raviv, K. Ewert, B. Jayna , J.B. Jones, H.P. Miller, L. Wilson and C.R. Safinya, Synchrotron X-ray diffraction study of microtubules buckling and bundling under osmotic stress: A probe of interprotofilament interactions, Physical Review Letters 93 (2004) 198104-1.

[79] W. Soedel, (1993) Vibrations of shells and plates, Marcel Dekker, New York.

[80] E. Ventsel and T. Krauthammer, (2004) Thin plates and shells, Marcel Dekker, Inc, New York.

[81] R.F. Gibson, (1994) Principles of composite material mechanics, McGraw-Hill, Inc, New York.

[82] A.K. Kaw, (2006) Mechanics of composite materials, Taylor & Francis, New York.

[83] B.I. Yakobson, C.J. Brabec and J. Bernholc, Nanomechanics of carbon tubes: Instabilities beyond linear response, Physical Review Letters 76 (1996) 2511.

[84] J. Schwaighofer and H.F. Microys, Orthotropic Cylindrical-shells under line load, Journal of Applied Mechanics (ASME) 46 (1979) 356.

[85] R.D. Zou and C.G. Foster, Simple solution for buckling of orthotropic circular cylindrical-shells, Thin-walled Structures 22 (1995) 143.

[86] P. Etitum and S.B. Dong, A comparative-study of stability of laminated anisotropic cylinders under axial-compression and tortion, Int. J. Solids & Struct. 32 (1995) 1231.

[87] C.Y. Wang, C.Q. Ru & A. Mioduchowski, Vibration of microtubules as orthotropic elastic shells, Physica E 35(1) (2006) 48.

[88] C.Y. Wang, C.Q. Ru, and A. Mioduchowski, Axisymmetric and beamlike vibrations of multiwall carbon nanotube, Physical Review B72, (2005) 075414-1.

[89] SP Timoshenko, DH Young & W. Weave, Vibration problems in engineering. New York. John Wiley (1974).

[90] M.E. Janson & M.A. Dogterom, Bending mode analysis for growing microtubules: Evidence for a velocity-dependent rigidity, Biophysical Journal 87 (2004) 2723.